

Responses to the Comments of Reviewer 1

(1) This study investigated the OH-oxidation of α -pinene ozonolysis products by reporting the mass yields and elemental composition of SOA produced. The main finding of this study is that OH-oxidation of α -pinene ozonolysis products that is equivalent of 2-4 days of atmospheric OH exposure leads to 20-40% net increase in the SOA yields and an increase in the aerosol O:C ratio by up to 0.04. While highlighting the importance of multi-generation aging in the atmospheric evolution of SOA, a topic that has been extensively studied previously, this finding alone, however, does not warrant the scientific significance and publication of this manuscript on ACP. Substantial revisions are needed, as described in the individual points below.

We address the various comments of the reviewer below. Our responses and corresponding changes in the paper follow each comment.

General:

(2) To what extent the experimental observations that 20-40% increase in SOA yields by further OH-oxidation could be applied to the actual atmospheric conditions? The authors used HONO as the OH precursor, which means that hundreds of ppbv levels of NO were present in the experiments conducted. Such an experimental condition is quite different from what is in the atmosphere, where most monoterpene emissions are from remote regions that encounter low NO air masses (e.g., a few ppb or less). As we know, NO significantly alters the VOCs oxidation mechanisms primarily by reacting with RO₂ radicals, leading to vastly different product distributions from those observed in the absence of NO, a chemical regime where RO₂+HO₂ and RO₂+RO₂ reactions dominate the fate of RO₂ radicals. That said, the experimental results presented in this study only represent a barely-seen scenario in the atmosphere and does not have any atmospheric relevance. The authors are suggested to conduct ‘low-NO_x’ experiments as well where H₂O₂, for example, can be used as the OH precursor. The observed increase in SOA yields, together with the high-NO experiments, can be used as upper and lower limits for the α -pinene SOA aging in the atmosphere.

Fundamentally, the issue of “atmospheric relevance” is one of whether the elementary chemical reactions occurring in the experimental system are the same as in the atmosphere. In this case, the question is the fate of peroxy radicals (RO₂). The chemical meaning of “high-NO_x” is “high-NO” in the sense that the dominant fate of RO₂ radicals is to react with NO. Therefore, by working at relatively high NO concentrations, we isolate the high-NO_x pathway for the aging reactions. This is the same as experiments using H₂O₂ photolysis, which typically have extremely high H₂O₂ concentrations and thus a large flux through the reaction $\text{OH} + \text{H}_2\text{O}_2 \rightarrow \text{H}_2\text{O} + \text{HO}_2$. Those experiments tend to isolate the RO₂ + HO₂ pathway. In general, it is an error to conflate “atmospherically relevant” with “atmospheric concentrations,” though it is important to establish that the rate-limiting chemistry is relevant to the atmosphere. We have added the above important point in the revised paper.

(2) The methodology of this study, including the chamber experimental approach, SOA yield measurements corrected by particle wall loss, O:C ratio calculations by AMS measurements, has been widely used in the community for decades. The main result of this study, i.e., SOA yields increase by 20%-40% upon OH-oxidation aging, is insufficient to warrant publication of this manuscript. The authors should endeavor to explore more detailed mechanisms involved in the α -pinene SOA aging by thoroughly analyzing the AMS data, e.g., What functionalities/products have changed and contributed to SOA production during aging? Any indication of PMF analysis, for example, on the key processes involved in the chemical aging?

PMF analysis works by separating the AMS-measured mass spectra into individual factors, and comparing those factors to existing libraries of mass spectra for the purpose of identifying potential sources for the SOA components. It is mostly used on ambient measurements where the sources for the OA are uncertain, while in these chamber experiments, we know that the SOA is formed via monoterpene oxidation. Application of this technique usually results in two or three factors with the fresh, aged and may be an intermediate product. While there could be useful information in this analysis it rarely provides the necessary chemical insights in cases where the changes in the spectra are relatively small like here.

In an attempt to explore the functionalities/products that may have changed during aging, we used the AMS high resolution family analysis. Each fitted ion is grouped into a “family” based on their chemical formula, and the families used are: CH, CHO, CHO₂, C_x, HO, and NO. These are the main components of the organics formed, with family HO calculated by subtracting the other families from the total organic signals, because sulfate can fragment into water and thus interfere with family HO. We used family NO to represent the organonitrate compounds formed during the aging step.

Based on the results for example of Experiments 1 and 2, the less oxidized ion family CH decreased around 10% during the aging process (from 41.9% to 38.1% of the OA in Exp. 1 and from 40.5% to 35.3% in Exp. 2) while the more oxidized components CHO₂ increased 4% in Exp. 1 (from 12.8 to 13.3%) and 16% in Exp. 2 (from 14.9% to 17.3%). The changes in the family CHO were +4% in Exp. 1 and -6% in Exp. 2 suggesting that there is both production and destruction of the corresponding family members. The organonitrate compounds as expected were close to zero initially in these experiments. In the end of the aging process the NO family represent 3-3.5% of the organic aerosol. There were less than 1 % C_x formed during the course of both experiments and their contribution stayed constant. This information has been added to the manuscript.

CO₂⁺ (m/z 44) from family CHO₂ and C₂H₃O⁺ (m/z 43) from family CHO are usually identified in aged and relatively fresh aerosols, respectively. Their fractions of the total organics, f_{44} and f_{43} , have been used as chemical indicators in chamber experiments (Donahue et al., 2012). During the dark ozonolysis period of Exp. 1, the f_{43} increased initially and stayed practically constant after t=0.2 h while f_{44} decreased. This indicates the majority of the SOA formed initially was fresh. After the first introduction of OH, both f_{43} and f_{44} showed a stepwise increase, indicating formation of relatively fresh SOA and oxidation of the SOA. After the second introduction of OH,

the f_{43} decreased while f_{44} increased over time until the end of the experiment, indicating the formed SOA was getting more oxidized with aging. During Exp. 2, the f_{43} increased sharply initially and then slowly decreased over the dark ozonolysis period. This is consistent with the “ripening” effect observed during the MUCHACHAS campaign (Donahue et al., 2012). Overall, f_{43} decreased while f_{44} increased over the course of Exp. 2, indicating formed SOA being oxidized during aging.

The above analysis has been added to the revised paper and the corresponding figures have been added to the Supplementary Information.

Specific:

(3) Page 2, Line 35-36: There have been a number of studies investigating the SOA aging processes using both static chamber and flow tube reactors (e.g., Robinson et al., Science, 2007; Loza et al., ACP, 2012; Lambe et al., ES&T, 2012). The authors need to revise the statement ‘Most laboratory studies of SOA formation so far have focused on the ...’

We have revised the corresponding sentence noting that the early SOA studies focused on the first stage of reactions.

(4) Page 3, Line 64: References need to be given here.

We have the corresponding three references at this point.

(5) Page 6, Line 154: What is the particle size range measured by SMPS?

The SMPS was set to measure particles from 15-700 nm for the experiments in this work. This information has been added to the paper.

(6) Page 6, Line 171: The OH radical molar yield from ozonolysis of a-pinene is roughly 0.7. So technically, the measured SOA yield at first stage is already a result of certain OH aging. Have the authors estimated the fraction of a-pinene that was oxidized by OH radical in the ozonolysis experiments? Have the authors considered adding any OH scavengers (e.g., H₂O₂, CO, methanol) in the first stage of the experiments?

This is a good point. OH scavengers cannot be used in the first phase of these aging experiments, because they will react with the OH in the second phase and will not allow the chemical aging to take place. As a result, the first phase of the experiment includes reactions of the precursor and to a limited extent of the first generation products with OH. We have used a kinetic box model of the system to estimate the extent of these reactions. Assuming a molar yield of 0.7 for a-pinene ozonolysis the model predicts that a little more than one third of the a-pinene reacted with OH in these experiments. Please note that these two reactions also take place together in the ambient atmosphere. This information has been added to the revised manuscript.

(7) Page 7, Line 205: The assumption that the particle loss rate in the 300-600 nm range is the same potentially leads to underestimation of the corrected SOA yields, as bigger particles have higher wall loss rate due to gravity deposition.

Gravitational settling predominantly affects particles bigger than 1 micrometer (Crump and Seinfeld, 1981; McMurry and Rader, 1985), while the majority of the particle mass in our experiments was in the range of 100-600 nm. We have regularly performed experiments with seed particles to characterize the k 's for the aforementioned size range and the loss constant does not vary in our chamber from 300 to 600 nm. The errors caused by using a constant fit for particles of 300-600 nm were evaluated by applying the same k 's to the seed loss periods during Exp. 1. The variability for the final seed loss period ($t=4.2-8.5$ h) was 4.2 %, indicating the corrected seed particle volume stayed relatively constant (Fig. 3). We have assumed the same uncertainty of 4.2 % for particles during the SOA formation. This explanation has been added to the paper.

(8) Page 8, Line 236: The authors are suggested calculate the SOA density from the AMS measured O:C and H:C ratio of SOA (Kuwata et al., ES&T, 2012) and compare with the current value used. An SOA density of $1.4 \mu\text{g m}^{-3}$ has been used in our calculations based on results from previous studies. We also used the Kostenidou et al. (2007) approach matching the AMS-mass/composition distribution with the SMPS measured volume distributions and estimated an average density of 1.3 g cm^{-3} .

(9) Page 9, Line 237-238: Adding the ' $V(t)/V_{\text{max}}$ ' factor in the SOA yield correction procedure does not seem necessary. The authors stated that 'deviations of $V(t)$ from V_{max} are caused by the uncertainty associated in applying the size dependent wall loss corrections'. As we know, particle wall loss rate depends on a few parameters, including chamber size, eddy diffusion, static charges on the Teflon surface, and etc. For most experiments presented here that only lasted for a few hours, these parameters should be fairly constant so that the particle wall loss rate should be quite consistent before and after one experiment. Where are the deviations originating from? I wonder if the assumption that particle loss rate in the 300-600 nm range is the same has any impact on the SOA yield correction here.

We defined the parameter, ε_V (Line 223), as an estimation for the uncertainties caused by our particle wall-loss correction. An ε_V of 4.2 % was calculated for Exp. 1 based on how much the loss-corrected seed volume ($t=4.2-8.5$ h) deviated from its average value. The deviation of $V(t)$ from V_{max} is likely caused by the uncertainty of our particle wall-loss correction, which is 4.2 % in this case, and may well include the effect of using a constant value for particles ranging in size of 300-600 nm. When calculating the corrected SOA volume, we have to subtract the seed from the corrected total volume concentration. With the goal in mind of minimizing the impact of the uncertainties caused by the particle loss correction on formed SOA, we introduced the ' $V(t)/V_{\text{max}}$ ' factor to attribute part of this 4.2 % error to the seed. If we subtract a constant seed volume, we are intrinsically attributing this 4.2 % error all and only to the corrected SOA and we get the lower limit of the corrected SOA volume.

(10) Page 27, Figure 5: Why the O:C ratio of SOA kept decreasing in the second dark period? What are the concentrations of NO_x and O₃ during this period? Is there any NO₃-initiated chemistry going on?

Similar evolution of the AMS spectra during periods without photochemistry has been observed in a number of similar studies. Donahue et al. (2012) called this evolution ripening to distinguish it from OH aging. The nature of this process is not well understood but it probably involves heterogeneous reactions. In our experiments the ozone concentration during this period was practically zero, so the production of NO₃ and the consecutive reactions were highly unlikely. We have added a short discussion and the corresponding reference to ripening in the paper.

Responses to the Comments of Reviewer 2

(1) In this manuscript the authors present results of a laboratory study in which they investigated the chemical aging of SOA formed from the ozonolysis of α -pinene. The aging was conducted by photolyzing HONO (to form OH radicals) that was added at two different times following completion of the ozonolysis reaction. The effects of aging were determined by monitoring the SOA mass using an SMPS and the composition using an AMS. Careful corrections were made for the effects of particle and vapor wall loss on the SOA yields. The results demonstrate that oxidation comparable to a few days of atmospheric aging lead to the formation of a significant amount of additional SOA mass, as well as small changes in composition as measured by the O/C ratio. The results are consistent with previous studies of this type, but are of to SOA yield corrections that are important in aging experiments. The experiments and data analysis were carefully done, and the manuscript is well written. I think the manuscript will be suitable for publication in ACP once the following comments have been addressed.

We address the various comments of the reviewer below. Our responses and corresponding changes in the paper follow each comment.

Specific:

(1) Page 14, Lines 407–410: It seems that this estimate of the effect of gas-wall partitioning of vapors on SOA formation assumes that all the first-generation products are either fully volatile or non-volatile with respect gas-particle partitioning. But for semi-volatile compounds the 15 min condensation time scale is also the upper limit to the time scale to achieve gas-particle partitioning equilibrium. In this case, some vapor will remain in the gas phase and continue to be lost to the chamber walls throughout the experiment because of the large effective particle mass of the walls. I think the approach used here thus provides only a lower-limit estimate to loss of vapors to the wall.

The reviewer is correct about our approach being the lower-limit estimate to vapor wall loss, and yet this is consistent with what we observed from the measurements. As indicated in Fig. 6, the organics to sulfate ratio stayed practically constant after its first peak at $t=0.7$ h until the introduction of OH. This is consistent with the fact that the SVOCs formed in our system only accounted for a small fraction of the products. This is also consistent with what Ye et al. (2015) observed for the α -pinene ozonolysis system. With a moderate precursor concentration (α -pinene <90 ppb), the SVOCs formed represented 20 % of the products. We have added this discussion to the paper.

(2) Page 14, Lines 408–410: It is not clear how the estimated loss of vapors to the walls is converted to an SOA yield correction.

Our zeroth-order correction simply assumes that the yields increase also by 6.3%. This results in a net increase of the yields of 1-3%. We have added this clarification to the paper.

(3) Page 15, Line 435–437: It would be straightforward to estimate the potential increase in O/C ratio due to heterogeneous oxidation by OH radicals and thus test this hypothesis.

Heterogeneous oxidation here refers to the uptake of OH by the SVOCs and the LVOCs in the condensed phase and the corresponding reactions that take place. Given that these reactions can be quite complex probably involving both functionalization and fragmentation the estimation of the expected O/C ratio is not straightforward.

(4) Page 15, Line 437: Why can't the observed changes in O/C ratio with aging be the result of gas-phase oxidation of semi-volatile compounds coupled to gas-particle partitioning, as proposed by Robinson et al. (2007), rather than heterogeneous oxidation?

Gas-phase reactions could of course contribute to the observed O/C ratio changes. However, the corresponding condensation of the products should result in a detectable increase in SOA concentration during the same period. We could not observe such a change; therefore, the contribution of gas-phase oxidation is probably small. Heterogeneous reactions can explain this significant change of O/C without a corresponding increase in SOA mass concentration. This explanation has been added to the paper.

(5) Page 16: The Conclusions section as is really just a brief summary of the results, written solely within the context of these experiments. I suggest the authors provide a broader discussion of the relevance of these results to studies of atmospheric SOA and what they contribute to knowledge of the formation, composition, and properties of SOA.

We have followed the suggestion of the reviewer and added a discussion of the relevance of these results for atmospheric SOA.

Multi-generation Chemical Aging of α -Pinene Ozonolysis Products by Reactions with OH

N. Wang¹, E. Kostenidou^{2,3}, N. M. Donahue¹ and S. N. Pandis^{1,2,3}

¹Department of Chemical Engineering, Carnegie Mellon University, Pittsburgh

²Department of Chemical Engineering, University of Patras, Patra, Greece

³Institute of Chemical Engineering Sciences (ICE-HT), FORTH, Patra, Greece

Abstract

Secondary organic aerosol (SOA) formation from volatile organic compounds (VOCs) in the atmosphere can be thought of as a succession of oxidation steps. The production of later-generation SOA via continued oxidation of the first-generation products is defined as chemical aging. This study investigates aging in the α -pinene ozonolysis system with hydroxyl radicals (OH) through smog chamber experiments. The first-generation α -pinene ozonolysis products were allowed to react further with OH formed via HONO photolysis. After an equivalent of 2-4 days' of typical atmospheric oxidation conditions, homogeneous OH oxidation of the α -pinene ozonolysis products resulted in a 20-40 % net increase of the SOA for the experimental conditions used in this work. A more oxygenated product distribution was observed after aging based on the increase in aerosol atomic oxygen to carbon ratio (O:C) by up to 0.04. Experiments performed at intermediate relative humidity (RH) of 50 % showed no significant difference in additional SOA formation during aging compared to those performed at low RH of less than 20 %.

1. Introduction

Anthropogenic activities such as fuel combustion as well as biogenic sources such as emissions from vegetation can introduce particles and particle precursors into the atmosphere. In most areas, about half of the submicron aerosol mass on average is composed of organic compounds (Zhang et al., 2007). Organic particles directly emitted to the atmosphere are traditionally defined as primary organic aerosol (POA), while those formed through atmospheric

29 reactions and condensation of species with corresponding volatility are secondary (SOA).
30 Atmospheric aerosols represent a significant risk to human health by causing respiratory problems
31 and heart attacks (Davidson et al., 2005; Pope et al., 2009). At the same time these particles
32 influence the climate of our planet ([Intergovernmental Intergovernmental](#) Panel on Climate Change,
33 2007).

34 Oxygenated OA with a high oxygen to carbon ratio (O:C) is often the most important
35 component of ambient OA suggesting the importance of atmospheric chemistry in the formation
36 and processing of OA (Zhang et al., 2007). ~~Most laboratory~~ Early studies of SOA formation ~~so far~~
37 have focused on the first stage of reactions involving the target precursor reacting with the chosen
38 oxidant. In the atmosphere, organic vapors and particles interact with oxidants for days and
39 therefore successive oxidation processes are inevitable.

40 Chemical aging refers to the subsequent stages of SOA formation and evolution due to the
41 production of later-generation products via oxidation of first-generation products by oxidants such
42 as OH free radicals (Donahue et al., 2006; Henry et al., 2012). Previous studies have explored
43 various forms of aging, including heterogeneous reactions of oxidants and aerosols (George et al.,
44 2008), oligomerization (Kalberer et al., 2006), photolysis of either gas or condensed-phase
45 products (Henry and Donahue, 2012), and homogeneous gas-phase oxidation by OH (Donahue et
46 al., 2012). Homogeneous gas-phase oxidation reactions appear to be in general much faster than
47 heterogeneous reactions, due to diffusion limitations of the latter (Lambe et al., 2009). The first-
48 generation oxidation reactions of most SOA precursors convert much less than 50 % of the
49 precursor to SOA, leaving more than half of the carbon still in the gas-phase. Additional oxidation
50 of these vapors can potentially contribute additional and more oxygenated SOA components.
51 These later-generation reactions have been proposed to be a major missing step connecting
52 chamber studies to field measurements.

53 Zeroth order parameterizations have been developed to model the chemical aging of semi-
54 volatile POA emissions in chemical transport models (Robinson et al., 2007). CTMs using these
55 schemes show improved performance in urban areas such as Mexico City (Tsimpidi et al., 2011),
56 but tend to over-predict OA in areas such as the southeastern United States where biogenic VOCs
57 dominate if chemical aging is assumed to be a major source of additional SOA (Lane et al., 2008).
58 As a result, the importance of aging of biogenic SOA as a source of SOA mass concentration
59 remains an issue of debate.

60 The ozonolysis of α -pinene ($C_{10}H_{16}$) is considered one of the most important global SOA
61 sources (Griffin et al., 1999). The system has been well characterized through smog chamber
62 experiments where researchers quantified its SOA yields under different conditions, explored the
63 reaction pathways and mechanisms, and identified its product distributions. Recent studies suggest
64 that there is significant potential for additional SOA formation from homogeneous gas-phase aging
65 by OH of the first-generation α -pinene oxidation products ([Donahue et al., 2012](#); [Müller et al.,
66 2012](#); [Chacon-Madrid et al., 2013](#)). Major identified products existing in gas phase such as
67 pinonaldehyde and pinonic acid can serve as SOA precursors and further react with OH.
68 Pinonaldehyde reacts with OH, with SOA mass yields up to 5 % under low- NO_x conditions and
69 20 % under high- NO_x conditions (Chacon-Madrid et al., 2013). Müller et al. (2012) demonstrated
70 the formation of 1,2,3-butanetricarboxylic acid (MBTCA), an SOA product of low volatility
71 identified in α -pinene ozonolysis, through the gas-phase OH oxidation of pinonic acid. They
72 reported an experimental yield of 0.6 % for MBTCA from the gas-phase OH oxidation of pinonic
73 acid, accounting for about 10 % of the total SOA formed. The proposed formation mechanisms of
74 MBTCA is a classic example of semi-volatile precursors going through oxidation and forming
75 products of lower volatility.

76 The Multiple Chamber Aerosol Chemical Aging Study (MUCHACHAS) explored the gas-
77 phase OH aging effects of the α -pinene ozonolysis products via experiments performed in four
78 different smog chambers (Donahue et al., 2012). They were able to isolate the aging effect by
79 using different OH sources (HOOH photolysis, HONO photolysis, TME ozonolysis), light sources
80 (sunlight, quasi-solar lamps, 350 nm UV lamps), and chambers of different design in size and
81 material (Teflon and aluminum). Almost in all experiments, additional formation of SOA (up to
82 55 %) and a more oxidized product distribution (increasing O:C) were observed after aging.
83 However, in one of the chambers, strong UV photolysis led to decreasing SOA mass
84 concentrations in experiments with low to moderate OH levels, $[OH] \leq 2 \times 10^6$ molecules cm^{-3}
85 (Henry and Donahue, 2012). These authors concluded that chemical aging involves a complex set
86 of interacting processes with competing functionalization (conserved C number with products of
87 lower volatility and higher oxidation states) and fragmentation (cleavage of C-bond with products
88 over a wide volatility range and higher oxidation states) of the various organic compounds. A 2D-
89 volatility basis set (2D-VBS) simulation based on these two pathways and a branching ratio
90 between them showed that homogeneous OH aging can potentially more than double the α -pinene

91 SOA mass concentration, after about a day's equivalent of typical atmospheric oxidation
92 conditions. Uncertainties such as "ripening" during which SOA volatility evolves but its mass
93 remains constant, UV photolysis and heterogeneous OH uptake can further complicate the aging
94 process.

95 Qi et al. (2012) also explored aging of the α -pinene ozonolysis system through smog
96 chamber experiments using HOOH as an OH source and studied the UV photolysis effect. They
97 observed a 7.5 % increase in the SOA volume concentration and an increase of 0.03 in the O:C
98 after aging. Minimum photolysis effect was reported for these experiments.

99 One complication of chamber experiments is the interaction of particles with chamber
100 walls. The wall-loss rate of particles is a function of particle size, charge distribution, chamber
101 geometry, turbulence, and electric field within the chamber (Crump and Seinfeld, 1981). In order
102 to quantify SOA yields from chamber experiments, it is important to correct for particle wall loss.
103 Recent findings that organic vapors in the chamber can be directly lost to the Teflon walls as well
104 further complicate the wall-loss correction process (Matsunaga and Ziemann, 2010; Zhang et al.,
105 2014). Krechmer et al. (2016) measured the loss rate of vapors formed in the chamber and found
106 the corresponding timescale to be 7-13 min. Ye et al. (2016) determined the vapor wall-loss
107 timescale in the Carnegie Mellon chamber used in this work to be around 15 min for semi-volatile
108 organic compounds.

109 Despite the consensus from the aforementioned chamber studies that gas-phase OH aging
110 of α -pinene ozonolysis products can contribute to additional SOA formation, there lacks
111 consistency in the extent to which the additional mass can form for different OH exposures. Part
112 of the problem is that the estimated amount of additional SOA formed from these long-lasting
113 aging experiments can be extra sensitive to the particle and the vapor wall-loss correction methods
114 deployed. The uncertainties at the end of a 10-hour long aging experiment during which most
115 particles are lost to chamber walls and the measured suspended mass is low can be relatively high.
116 In this work, we aim to quantify the additional SOA formed during the aging step comparing
117 measurements from a suite of instrumentation. We adopt a size-dependent particle wall-loss
118 correction method and develop a procedure to better constrain the associated errors. We also
119 attempt to constrain the vapor loss using both theoretical calculations and measurements.

120

121

122

123 2. Experimental approach

124 We conducted experiments in a 12 m³ Teflon (Welch Fluorocarbons) smog chamber at
125 Carnegie Mellon University (CMU). The reactor was suspended in a temperature-controlled room
126 with walls covered with UV lights (GE 10526 and 10244). Prior to each experiment, we flushed
127 the chamber overnight with purified air under UV illumination to remove any residual particles
128 and gas-phase organics. We generated purified air by passing ambient air through a high-efficiency
129 particulate air (HEPA) filter to remove particles, an activated carbon filter to remove any organics,
130 a Purafil filter to remove NO_x, and finally a silica gel filter, keeping relative humidity (RH) below
131 5 % in the chamber before each experiment.

132 We pumped an ammonium sulfate solution (1 g L⁻¹) into the chamber at the beginning of
133 each experiment through an atomizer (TSI, model 3076) at a constant rate of 90 mL h⁻¹ to produce
134 droplets. The droplets passed through a diffusion dryer and a neutralizer to produce dry ammonium
135 sulfate seed particles. We injected seeds with a number mode size of 110 nm until they reached a
136 number concentration of 2×10⁴ cm⁻³, resulting in an initial seed mass concentration of around 40
137 μg m⁻³ and a surface area concentration of up to 1000 μm² cm⁻³. Typical organic vapors with a
138 molar weight of 250 g mol⁻¹ thus had an initial collision frequency with these seeds of 0.01 s⁻¹. We
139 injected α-pinene (Sigma-Aldrich, ≥ 99 %) into the chamber using a septum injector with purified
140 air as carrier flow. We generated ozone using a corona-discharge ozone generator (AZCO,
141 HTU500AC) to initiate the ozonolysis reaction. We prepared a fresh HONO solution in a bubbler
142 by adding a 4.9 g L⁻¹ sulfuric acid solution to a 6.9 g L⁻¹ sodium nitrite solution. We then turned
143 on the UV lights to start the photo-dissociation of HONO, producing OH.

144 At the end of each experiment, we injected additional ammonium-sulfate seeds into the
145 chamber using the same method with a more concentrated solution (5 g L⁻¹) in order to characterize
146 the particle wall-loss rates a second time.

147 We added butanol-d9 (Cambridge Isotope Laboratories, 98 %) into the chamber through
148 the septum injector as an OH tracer before the reaction started and used the method described in
149 Barnet et al. (2012) to calculate the OH produced by HONO photolysis. The OH concentration in
150 these experiments was around 2.4×10⁷ molecules cm⁻³ for the first hour, then dropped to around
151 5×10⁶ molecules cm⁻³ afterwards. The introduction and photolysis of HONO produces into the
152 chamber can bring in hundreds of ppb of NO_x, and thus the aging reactions in this work occurred

153 under high NO_x conditions; where the majority of the peroxy radicals during the aging step reacted
154 with NO during the aging phase of the experiments.

155 We performed experiments at both low RH of less than 20 % and intermediate RH of 50 %.
156 To add water vapor to the chamber, we used a stream of purified air to carry ultrapure water
157 (Millipore water purification system) in a bubbler into the chamber before the introduction of seeds.

158 We measured the particle size distribution using a TSI Scanning Mobility Particle Sizer,
159 SMPS (classifier model 3080; CPC model 3010 or 3772), with flows adjusted to measure particle
160 diameters in the size range of 15-700 nm range. ~~and~~ We measured the particle composition and mass
161 spectrum of the OA with an Aerodyne High Resolution Time-of-flight Aerosol Mass Spectrometer
162 (HR-ToF-AMS). We monitored the concentrations of α -pinene and butanol-d9 using a Proton
163 Transfer Reaction-Mass Spectrometer (PTR-MS, Ionicon), the ozone concentration using a Dasibi
164 1008 ozone monitor (ICE: Teledyne 400E), and NO_x (NO + NO₂) levels using a Teledyne API
165 NO_x Analyzer 200A (ICE: Teledyne T201). We held the chamber temperature constant at 22 °C
166 throughout all experiments. We list the initial conditions of the experiments performed for this
167 work in Table 1.

169 3. Data analysis

170 3.1 SOA yields

171 The SOA mass yield, Y , is a metric of the ability of a gaseous precursor to form SOA, and
172 is defined as $Y = C_{\text{SOA}}/\Delta\text{VOC}$, where C_{SOA} is the produced SOA mass concentration (in $\mu\text{g m}^{-3}$)
173 and ΔVOC the amount of the VOC precursor (α -pinene in this case) reacted (in $\mu\text{g m}^{-3}$). To
174 separate the effect of aging on SOA mass concentration, we define a first-generation SOA mass
175 yield, $Y_1 = C_{\text{SOA},1}/\Delta\text{VOC}$, and a second-generation SOA mass yield, $Y_2 = C_{\text{SOA},2}/\Delta\text{VOC}$. $C_{\text{SOA},1}$ and
176 $C_{\text{SOA},2}$ are the concentrations of SOA formed before, and after aging with hydroxyl radicals. All
177 α -pinene reacts away during the first stage and thus ΔVOC for the second stage is the same as the
178 initial α -pinene concentration in the chamber.

180 3.2 Particle wall-loss correction

181 In this work, we try to reduce the uncertainties in the estimated SOA mass concentration
182 associated with the particle wall-loss correction. This uncertainty can be significant due to two
183 aspects of these aging experiments: the evolution of the particle size distribution and the duration

184 of the experiments. In these aging experiments, where particles grow by condensation and
185 coagulation for several hours, the particle size distribution can potentially shift, covering a wide
186 size range over the course of an experiment. Particle wall losses are size dependent, and this shift
187 can introduce significant errors if a constant loss rate constant is assumed. To minimize these
188 problems, we adopted a size-dependent particle wall-loss correction method where we determined
189 the particle wall-loss rate constant, k , at each particle size, D_p .

190

191 3.2.1 Determination of particle wall-loss rate constants

192 The size-dependent particle wall-loss correction method (Keywood et al., 2004; Ng et al.,
193 2007; Loza et al., 2012; Nah et al., 2016) adopted in this work is based on the SMPS-measured
194 particle size distribution. At each particle size bin i , the first-order particle wall-loss rate constant
195 k , can be determined as the slope of the following equation:

196

$$197 \ln[N_i(t)] = -k_i t + Q \quad (1)$$

198

199 where $N_i(t)$ is the SMPS-measured aerosol number concentration at size bin i and Q is an arbitrary
200 constant. Applying Eqn. 1 across the entire SMPS-measured particle size range, we obtain the
201 particle wall-loss rate constant function, $k(D_p)$.

202 To determine the $k(D_p)$ profile, we utilized the initial four-hour ammonium sulfate seed
203 wall-loss period for each experiment. Since k may also vary with time (McMurray and Rader,
204 1985), we determined a second $k(D_p)$ profile for each experiment using the ammonium sulfate
205 seed wall-loss period at the end. It is important to ensure that the k 's, especially at sizes where the
206 majority of SOA mass is distributed, remain the same over the course of each experiment.

207 The $k(D_p)$ -values calculated (with an $R^2 > 0.5$) based on SMPS measurements of the seed
208 distribution from this work usually only cover particle size range of 30-300 nm due to the lack of
209 particles at either end of the particle size distribution. To determine the $k(D_p)$ -for $D_p < 30$ nm, we
210 use a simple log-linear fit of k 's from 30-50 nm and back extrapolate it to 10 nm. To determine
211 $k(D_p)$ for $D_p > 300$ nm, we assume that the constant is practically the same in the 300-6700 nm
212 range. We confirmed this with additional seed-only experiments where there were enough particles
213 at that size range (Wang et al., 2017). [Significant increases of the rate loss constant are observed
214 for particles larger than 1 \$\mu\$ m, while in our experiments the particles remained small than 600 nm](#)

or so. A measure of the uncertainty of these corrections is the variability of the corrected mass concentration during the seed wall-loss periods as discussed in the next section. The uncertainty created by using the fits were determined by applying the same $k(D_p)$ profile to the seed wall-loss periods in each experiment and evaluating how much the corrected seed number/volume concentration varied (Sec. 3.2.2). We then applied the complete $k(D_p)$ profile to correct for the particle number and mass concentration. Details regarding the wall-loss profiles in the CMU chamber and the execution of the size-dependent particle wall-loss correction for this work can be found in Wang et al. (2017).

3.2.2 Correction of SMPS measurements

The corrected particle number concentration at each size bin i , $N_i(t)$, can be calculated numerically,

$$N_i(t) = N_i^m(t) + k_i \int_0^t N_i^m(t) dt, \quad (2)$$

from the measured values $N_i^m(t)$ and the $k(D_p)$ corresponding to the size bin i , k_i .

For closed systems in which coagulation is slow, the particle wall-loss corrected number concentration should be constant. In order to evaluate how well the correction works, we define the parameter: $\varepsilon_N = 2\sigma_{N_s} / \overline{N_s}$, where σ_{N_s} is the standard deviation of the particle wall-loss corrected number concentration for the seed wall-loss periods and $\overline{N_s}$ the average. Similarly, we define $\varepsilon_V = 2\sigma_{N_s} / \overline{V_s}$ based on the particle wall-loss corrected volume concentration for the two seed wall-loss periods. Only when all four values, ε_N and ε_V for both the initial and the final seed periods, are less than 5 % do we deem the particle wall-loss correction valid for that individual experiment. Experiments in which these criteria were not met were not included in the analysis.

To calculate the mass concentration of the formed SOA, C_{SOA} , during the course of an experiment, we treated the particle wall-loss corrected aerosol volume concentration $V(t)$ differently before and after its maximum, V_{max} . For

$$\begin{aligned} t < t_{V_{max}}, C_{SOA}(t) &= (V(t) - V_s) \rho_{SOA}, \\ t \geq t_{V_{max}}, C_{SOA}(t) &= [V(t) - V_s \frac{V(t)}{V_{max}}] \rho_{SOA}, \end{aligned} \quad (3)$$

245
246 where $t_{V_{max}}$ is the corresponding time at the maximum particle wall-loss corrected total aerosol
247 volume concentration. V_s is the average particle wall-loss corrected seed volume concentration
248 before the beginning of each experiment. ρ_{SOA} is the SOA density, assumed to be equal to $1.4 \mu\text{g}$
249 m^{-3} (Kostenidou et al., 2007). Ideally, $V(t)$ should equal to V_{max} after the reactions are completed
250 and particle wall loss is the only process after $t_{V_{max}}$. However, deviations of $V(t)$ from V_{max} are
251 caused by the uncertainty associated in applying the size-dependent wall-loss corrections. By
252 scaling V_s with $V(t)/V_{max}$, we are distributing the impact of any potential fluctuations in $V(t)$ evenly
253 to both the seeds and the organics, and thus obtain a more stable C_{SOA} after aging.

254 255 **3.3 Analysis of AMS measurements**

256 ——— The HR-AMS was operated in V mode during the experiments in this work. Squirrel
257 v1.56D was used to analyze the data. The atomic oxygen to carbon ratio, O:C, was determined
258 based on the unit-resolution correlation described in Caragaratna et al. (2015). Nitrate signals were
259 attributed to organics since the only sources of them in these experiments are organonitrate
260 compounds.

261 In an attempt to explore the functionalities/products that may have changed during aging,
262 we used the AMS high-resolution (HR)-family analysis. We used Pika 1.15D to analyze the HR
263 data, with HR ions fitted to m/z 200. Each fitted ion is grouped into a “family” based on their
264 chemical formula, and the families used are: CH, CHO, CHO₂, C_x, HO, and NO. These are the
265 main components of the organics formed, with family HO calculated by subtracting the
266 concentrations of the other families from the total organic signal. This is necessary because the
267 fragmentation of sulfates can fragment into water and thus interfere with the family HO. FWe used
268 family NO can be used to represent the organonitrates compounds formed during the aging phase
269 of the experiments step.

270 271 **4. Results and discussion**

272 The particle wall-loss corrected aerosol number concentration evolution during a typical
273 experiment (Exp. 1) together with the SMPS raw measurements are shown in Fig. 1. Prior to the
274 ozonolysis, $18,000 \text{ cm}^{-3}$ ammonium sulfate particles were added to the chamber as seeds. After a
275 4.5 h wall-loss period, $8,000 \text{ cm}^{-3}$ particles remained suspended, serving as pre-existing surface

276 for condensation. At $t=0$, ozone was added into the chamber, reacting with α -pinene to form
277 condensable first-generation products. The ozonolysis of α -pinene has been found to produce
278 OH with a molar yield of approximately ~ 0.7 (Paulson et al., 1998), which in our experiments
279 resulted in approximately a little more than one third of the precursor reacting with OH. An
280 additional 100 cm^{-3} particles were formed due to nucleation at this time. Two doses of HONO
281 were added into the chamber in this experiment at $t=0.4 \text{ h}$ and $t=1.3 \text{ h}$, respectively. HONO was
282 allowed to mix in the chamber and then the UV lights were turned on at $t=0.8 \text{ h}$ and $t=1.8 \text{ h}$ to
283 produce OH. At $t=3.5 \text{ h}$, another $10,000 \text{ cm}^{-3}$ ammonium sulfate particles were added into the
284 chamber for a second 4 h long determination of the $k(D_p)$ profile for this experiment.

285 The two $k(D_p)$ profiles determined from the initial seed wall-loss period and the one at the
286 end of the experiment are shown in Fig. 2. They agree relatively well with small discrepancies at
287 $D_p < 50 \text{ nm}$. The complete $k(D_p)$ profile used for the size-dependent particle wall-loss correction
288 is also shown.

289 As indicated in Fig. 1, the particle wall-loss corrected aerosol number concentration
290 remains relative level at $t < 0 \text{ h}$ and $t > 3.5 \text{ h}$, with $\varepsilon_{N,1} = 3.3 \%$ and $\varepsilon_{N,2} = 0.5 \%$, respectively. The
291 particle wall-loss corrected aerosol volume concentration (Fig. 3) at the initial seed wall-loss
292 period and that at the end had variabilities equal to $\varepsilon_{V,initial} = 4.2 \%$ and $\varepsilon_{V,end} = 3.8 \%$,
293 respectively. All parameters were less than 5 % and therefore the accuracy of the wall-loss
294 correction was acceptable.

295 The particle wall-loss corrected aerosol volume concentration evolution for Exp. 1 together
296 with the corresponding SMPS raw measurements are shown in Fig. 3. Particles grew from $t=0$ to
297 0.7 h and $t=0.8$ to 1 h due to vapor condensation. The total aerosol volume peaked at $t=0.7 \text{ h}$ during
298 the first-generation oxidation, and reached its maximum at $t=1.1 \text{ h}$ due to aging during the second-
299 generation oxidation. The change in volume during the second addition of OH at 1.7 h was
300 negligible.

301 The SOA mass concentration evolution for Exp. 1 calculated using Eqn. 3 is shown in Fig.
302 4. The error bars are calculated using the highest ε (in this case $\varepsilon_{V,1} = 4.2 \%$). For this experiment,
303 $37.7 \pm 1.6 \mu\text{g m}^{-3}$ of SOA was formed during ozonolysis. An additional $11.1 \pm 2.6 \mu\text{g m}^{-3}$ SOA was
304 formed during the first aging period. The SOA reached $48.8 \pm 2 \mu\text{g m}^{-3}$ after aging and remained
305 approximately constant until the end of the experiment. The total SOA produced and the calculated
306 SOA yields for all experiments are listed in Table 2.

307 The AMS-derived atomic oxygen to carbon ratio (O:C) evolution for Exp. 1 is shown
308 together with the AMS-measured aerosol composition (assuming CE=1) in Fig. 5. The increase in
309 the sulfate signals at $t=0$ is caused by a change in the instrument collection efficiency. Due to the
310 uncertainty caused by CE changes over the course of an experiment, we did not use the absolute
311 AMS-measured organic mass concentration for any quantitative analysis. Using the algorithm
312 derived by Kostenidou et al. (2007), we calculated the CE to be ~ 0.25 for the initial seed period
313 and ~ 0.4 after the seeds were coated with organics. A quick check comparing the two stepwise
314 increase in the CE-corrected organic mass concentration to those derived from SMPS revealed that
315 the results from both instrument agreed reasonably well. The algorithm also predicted/estimated
316 that the SOA density was to be $1.3 \pm 0.15 \text{ g cm}^{-3}$, in good agreement with the Kuwata et al. (2012)
317 parameterization based on the measured O:C and H:C which also predicted 1.3 g cm^{-3} .
318 which we cross-checked with the method based on the O:C and the H:C from Exp. 1
319 (Kuwata et al., 2012).

320 The O:C is a collective measure for the ongoing chemistry during these aging experiments.
321 In Exp. 1, the O:C kept decreasing due to the freshly-formed semi-volatile SOA condensing onto
322 particles from $t=0$ to 0.5 h. Later during in the dark period (From $t=0.5$ h to 0.8 h (UV on), the O:C
323 ratio kept decreasing to 0.42 while the organic mass concentration stayed almost constant. This is
324 consistent with the “ripening” phenomenon, first observed during the MUCHACHAS campaign,
325 where the composition of the formed SOA keeps evolving after α -pinene has reacted while the
326 change in SOA mass is minimal (Tritscher et al., 2011). The nature of this process is not well-
327 understood, but it probably involves heterogeneous reactions. After OH radicals were generated
328 in the chamber at $t=0.8$ h, the semi-volatile vapors got oxidized to form second-generation products
329 of lower volatility, resulting in an increase of 0.02 in O:C in about 10 min. After $t=1$ h, the O:C
330 remained relatively constant but it started to decrease at $t=1.25$ h when the UV lights were turned
331 off. Since aging is a complex process that involves functionalization, fragmentation and
332 heterogeneous reactions, the trends in O:C are indicative of the competition among these processes.
333 The decrease we observed here was associated with turning the UV lights off, and thus it is likely
334 that some chemistry was perturbed and thus the processes resulting in decreasing O:C took over.
335 The decrease in O:C associated with turning off the UV lights was not consistent across the five
336 experiments. This further proves that this phenomenon is the result of several competing process
337 and needs further investigation on a molecular level. An inflection point at $t=1.7$ h was observed

338 after a second dose of OH being introduced in the chamber. Instead of the stepwise increase like
339 the one observed after the first dose of OH, the O:C increased slowly but steadily this time until
340 the end of the experiment to 0.45 with no significant increase in organic mass. This is also quite
341 consistent with what was observed in MUCHACHAS.

342 We used the organic to sulfate ratio (Org/Sulf) derived from AMS measurements to look
343 at the SOA formation in these experiments due to its insensitivity to changes in collection
344 efficiency. The Org/Sulf time series for Exp. 1 is shown in Fig. 6. The ratio increased to 1.25 at
345 $t=0.7$ h as the result of the first-generation vapors condensing onto pre-existing particles. After we
346 first turned on the UV lights, a stepwise increase in the ratio was observed and reached the
347 maximum value of 1.60 at $t=1.1$ h as a result of the second-generation oxidation chemistry. After
348 that, the ratio kept decreasing. A small bump was observed after the second introduction of OH
349 and then the ratio kept decreasing. One possible explanation for this continuous decrease is the
350 effect of the size-dependent particle wall-loss process. The faster removal of smaller particles
351 (which contain more SOA than sulfate) than that of the bigger ones (which have a lower SOA to
352 sulfate ratio) can lead to a decrease of the overall organic to sulfate ratio. Fig. 7 shows the size
353 dependence of the Org/Sulf, together with the mass distribution of both organic and sulfate for
354 Exp. 1. The Org/Sulf decreased dramatically from 10 to 1 over the particle vacuum aerodynamic
355 diameter (D_{va}) range of 200 – 500 nm, indicating strong composition dependence on particle size.
356 Since the majority of the mass is distributed in this range, the size-dependent particle wall-loss rate
357 can contribute significantly to the decrease observed in Fig. 6 after the Org/Sulf reached its
358 maximum.

359

360 **4.1 Effect of size-dependent losses on the organic to sulfate ratio**

361 To quantify the effect of the size-dependence of the particle wall-loss process on the
362 organic to sulfate ratio, we discretized the AMS-measured mass distribution $M(D_p)$ into 10 bins
363 in the particle diameter space and defined a mass-weighted particle wall-loss rate constant for each
364 species j , \bar{k}_j , as

365

$$366 \quad \bar{k}_j = \sum_{i=1}^{10} M_{ij} k_i / \sum_{i=1}^{10} M_{ij} \quad (4)$$

367

368 where M_{ij} is the aerosol mass concentration of species j for size bin i and k_i is the averaged $k(D_p)$
 369 across size bin i . Note that the particle diameter used in this section refers to the SMPS-measured
 370 mobility equivalent diameter D_p . The particle vacuum aerodynamic diameters derived from the
 371 AMS measurements have been converted to D_p using an SOA density of $1.4 \mu\text{g m}^{-3}$.

372 From Eqn. 4 we are able to determine a mass-weighted particle wall-loss rate constant for
 373 sulfate, \bar{k}_{SO_4} , and for organics, \bar{k}_{Org} . For the period after completion of the reactions and if there
 374 are only particle losses to the walls the Org/Sulf ratio should satisfy:

$$375 \quad (Org/Sulf)(t) = (Org/Sulf)_m(t) \exp(\bar{k}_{SO_4} - \bar{k}_{Org})t \quad (5)$$

376
 377 where $(Org/Sulf)_m(t)$ is the AMS-measured and $(Org/Sulf)(t)$ the loss-corrected organic to
 378 sulfate ratio.

380 We can test if indeed the particle wall losses are responsible for the decreasing ratio in Exp.
 381 1 focusing on the period from $t_1 = 1.2$ h to $t_2 = 1.7$ h (Fig. 6). In this example t_1 corresponds to
 382 the maximum Org/Sulf and t_2 is the second time in which the UV lights were turned on. Applying
 383 Eqn. 4, we found the mass-weighted particle wall-loss rate constant for organics, $\bar{k}_{Org} = 0.06 \text{ h}^{-1}$,
 384 and for sulfate, $\bar{k}_{SO_4} = 0.05 \text{ h}^{-1}$. The black line in the inset graph of Fig. 6 indicates the particle
 385 wall-loss corrected Org/Sulf for the chosen time period using Eqn. 5. The loss-corrected ratio
 386 remained relatively constant indicating that the size-dependent particle wall-loss process coupled
 387 with the different size distributions of the sulfate and organics were causing the decrease in the
 388 ratio. This exercise was repeated for the other experiments arriving in the same conclusion.

389

390 **4.2 Effect of chemical aging on additional SOA formation**

391 To quantify aging effects based on the SMPS measurements, we define the fractional
 392 change in the particle wall-loss corrected SOA mass concentration after aging, $\Delta[OA]$, as:

$$393 \quad \Delta[OA] = (C_{SOA,2} - C_{SOA,UV})/C_{SOA,1}, \quad (6)$$

394
 395 where $C_{SOA,UV}$ is the particle wall-loss corrected aerosol mass concentration at the time when we
 396 first turned on the UV lights. $C_{SOA,UV}$ can be equal to $C_{SOA,1}$ depending on how level the first-

398 generation SOA mass concentration remains after wall-loss correction. Fig. 8 summarizes the
399 $\Delta[\text{OA}]$ for all five experiments with the values and corresponding errors listed in Table 2. The OH
400 exposure resulted in an average increase of 24 ± 6 % in SOA mass concentration after aging, ranging
401 from 20 to 29 %. Our HONO injection method creates OH levels of about 2.4×10^7 molecules
402 cm^{-3} for the first hour and then the concentration dropped to around 5×10^6 molecules cm^{-3} . The
403 OH exposure is equivalent to 2-4 days of typical atmospheric oxidation conditions, assuming an
404 OH concentration of 2×10^6 molecules cm^{-3} . The uncertainties displayed in Fig. 8 were propagated
405 from uncertainties in the SOA mass concentration.

406 To quantify aging effects based on the AMS data, we define the fractional change in the
407 organic to sulfate ratio:

$$408 \Delta[\text{Org/Sulf}] = ([\text{Org/Sulf}]_2 - [\text{Org/Sulf}]_{\text{UV}}) / [\text{Org/Sulf}]_1, \quad (7)$$

410 where $[\text{Org/Sulf}]_{\text{UV}}$ refers to the organic to sulfate ratio at the time when we first turned on the UV
411 lights, $[\text{Org/Sulf}]_1$ the maximum before we first turned on the UV lights and $[\text{Org/Sulf}]_2$ the
412 maximum after the OH exposure. Fig. 8 summarizes the $\Delta[\text{Org/Sulf}]$ calculated for all five
413 experiments with the values and corresponding errors listed in Table 2. The uncertainties are based
414 on the deviation between the measured and the corrected Org/Sulf (Fig. 6 inset) over the chosen
415 time period. An associated error is calculated respectively for $[\text{Org/Sulf}]_{\text{UV}}$, $[\text{Org/Sulf}]_1$ and
416 $[\text{Org/Sulf}]_2$. The reported error for $\Delta[\text{Org/Sulf}]$ in Table 2 is the propagated results of the three.
417 For experiments in this work, the percent increase in organic to sulfate ratios ranged from 18 to
418 27 % with an average increase of 21 ± 4 %. The values are fairly consistent with the SMPS-derived
419 $\Delta[\text{OA}]$.

420

421 **4.2.1 Role of RH**

422 Exp. 5, performed at the intermediate RH of 50 %, resulted in a comparable change in SOA
423 formation after aging as experiments at lower RH (Fig. 8). In this experiment, the increase in
424 Org/Sulf after aging was 21.2 %, 1.5 % higher than the average $\Delta[\text{Org/Sulf}]$ of experiments 2-4.
425 $\Delta[\text{OA}]$ for Exp. 5 was 20.5 %, about 2 % lower than the average $\Delta[\text{OA}]$ of experiments 2-4. The
426 effect of RH on the SOA formation during chemical aging, at least for these conditions, appears
427 to be small.
428

429

430 4.2.2 Role of organic vapor loss to the Teflon walls

431 For chamber SOA experiments with preexisting particles, the particles act as competing
432 surface against the chamber walls. We calculated the condensation sink (CS) of particles using the
433 method described in Trump et al. (2014) with a unit accommodation coefficient, consistent with
434 recent findings (Julin et al., 2014; Palm et al., 2016). The calculated condensation sink in the form
435 of time scale for vapors condensing onto particles ($1/CS$) for Exp. 1 is shown in Fig. 9. During the
436 entire experiment, the timescale for vapors to condense onto particles remained less than a minute.
437 Compared to the organic vapor wall-loss timescale of 15 min in the CMU chamber (Ye et al.,
438 2016), the vapors condense onto the particles 15 times faster than that onto the walls. This
439 corresponds to a 6.3 % loss of the semi-volatile vapors to the walls. Assuming the yields for For
440 the experiments conducted in this work also increase by 6.3 %, the absolute yields should be
441 increased by 1-3 % after accounting for the vapor wall-loss effect. This approach is a conservative
442 estimation of vapor wall loss, and yet the results are consistent with what we observed from the
443 measurements. As indicated in Fig. 6, the organic to sulfate ratio stayed practically constant after
444 its first peak at $t=0.7$ h until the introduction of OH. This is consistent with the fact that the semi-
445 volatiles formed in our system only accounted for a small fraction of the products. Ye et al. (2016)
446 studied the SVOCs formed in the α -pinene ozonolysis system and found 20 % SVOCs in the
447 products formed from experiments with moderate precursor concentration (α -pinene=75 ppb).
448 They also observed that the SVOC fraction increased with increased amounts of reacted α -pinene.
449 Since the reacted α -pinene in our experiments ~~were~~ was less than 35 ppb, our observation of small
450 amount of SVOCs forming is also consistent with their results.

451 The situation is a little more complex for the second-generation oxidation because material
452 with higher volatilities that could have become SOA were lost during the time after the end of the
453 first phase and before the beginning of the second. To address this issue, OH radicals were
454 introduced about an hour earlier in Exp. 1 as compared to the rest of the experiments. A shorter
455 timescale ensures the first-generation vapor products react efficiently with OH instead of
456 interacting with the chamber walls as in the case of longer timescales. There was an increase of
457 27 % in Org/Sulf in this experiment after aging, 7 % more than the average of the other four
458 experiments. $\Delta[OA]$ for Exp. 1 was 29.4 %, about 7.5 % higher than the average of the rest four
459 experiments. If we attribute this 7 % difference purely to the vapor wall-loss effect, then we

460 estimate that vapor losses can increase the additional SOA formation by roughly another 10 % for
461 the experiments conducted in this work.

462

463 **4.3 Effect of chemical aging on O:C aerosol composition**

464 Fig. 10 summarizes the absolute increase in O:C after the two doses of OH, respectively,
465 with the corresponding exposure required to achieve the increase. As we discussed above using
466 Exp. 1 as an example, the O:C in all experiments showed a stepwise increase after the first OH
467 introduction while it grew continuously after the second OH introduction until the end of the
468 experiment. For these five experiments, it took 10 - 30 min for the O:C to increase by 0.02-0.04.
469 The stepwise increase in O:C is caused by the rapid reactions between the first generation vapor
470 products and the OH. One of the major products identified in the gas phase from the α -pinene
471 ozonolysis system, pinonaldehyde, reacts with OH at a rate of $4.4 \times 10^{-11} \text{ cm}^3 \text{ molecule}^{-1} \text{ s}^{-1}$
472 (Atkinson and Arey, 2003). During the first hour of OH introduction, the OH concentration
473 remains on average at a steady state of $2.4 \times 10^7 \text{ molecule cm}^{-3}$. A quick estimation of
474 $1/k_{OH}[OH]$ gives a timescale of 16 min, which is consistent with what we observed in these
475 experiments.

476 The second exposure corresponds to the period until the end of each experiment. The
477 increase in O:C of 0.01 to 0.04 during this stage clearly indicates change in SOA composition,
478 however paired with minimum change in SOA mass. Although gas-phase reactions can contribute
479 to these observed changes in O:C, the corresponding condensation of the products should also
480 result in a detectable increase in SOA concentration during the same period. Given that changes
481 in SOA concentration could not be detected the contribution of gas-phase oxidation was probably
482 small. -In addition, we observed small amounts of SVOCs forming in our system as discussed
483 above. Therefore, the contribution of gas-phase oxidation was probably small. And our observation
484 of the significant change in O:C without corresponding increase in SOA mass concentration This
485 phenomenon is was likely caused by heterogeneous reactions.

486 Based on the HR family analysis results, for example, of Exp. 1 (Fig. S1) and Exp. 2 (Fig.
487 S3), the less oxidized ion family CH decreased around 10 percent during the aging process (i.e.,
488 from 41.9 to 38.1 percent of the OA in Exp. 1 and from 40.5 to 35.3 percent in Exp. 2) while the
489 more oxidized components CHO₂ increased 4 percent in Exp. 1 (from 12.8 to 13.3 percent) and 16
490 percent in Exp. 2 (from 14.9 to 17.3 percent). The changes in the family CHO were +4 percent in

491 Exp. 1 and -6 percent in Exp. 2, suggesting that there were both production and destruction of
492 the corresponding family members. The concentration of organonitrates compounds was, as
493 expected, were close to zero initially in these experiments. At the end of the aging process, the NO
494 family represented 3-3.5 percent of the OA.

495 CO₂⁺ (m/z 44) from family CHO₂ and C₂H₃O⁺ (m/z 43) from family CHO are usually
496 identified in aged and relatively fresh aerosols, respectively. Their fractions of the total organics,
497 f₄₄ and f₄₃, have been used as chemical indicators in chamber experiments (Donahue et al., 2012).
498 During the dark ozonolysis period of Exp. 1 (Fig. S2), the f₄₃ increased initially and stayed
499 practically constant after t=0.2 h, while f₄₄ decreased. This indicates the majority of the SOA
500 formed initially was fresh. After the first introduction of OH, both f₄₃ and f₄₄ showed a stepwise
501 increase, indicating formation of relatively fresh SOA and oxidation of the SOA. After the second
502 introduction of OH, the f₄₃ decreased while f₄₄ increased over time until the end of the experiment,
503 indicating that the e formed SOA was getting progressively more oxidized during aging. During
504 Exp. 2 (Fig. S4), the f₄₃ increased sharply initially and then slowly decreased during over the dark
505 ozonolysis period. This is consistent with the “ripening” effect observed during the
506 MUCHACHAS campaign (Donahue et al., 2012). Overall, f₄₃ decreased while f₄₄ increased over
507 the course of Exp. 2, indicating that the initially formed SOA was getting more being oxidized
508 during aging.

509 510 **4.4 Comparison with other studies**

511 Overall, the results from our chamber experiments in this work are consistent to those from
512 the MUCHACHAS chambers. After adopting a size-dependent particle wall-loss correction
513 method, we observed 20-30 % additional SOA formation after aging. Vapor wall-loss effect can
514 account for an additional 10 %, increasing the range to 20-40 %. The O:C presented a stepwise
515 increase of 0.02-0.04 after the first introduction of OH, and then increased gradually overtime after
516 the second introduction of OH.

517 During the MUCHACHAS campaign, mixtures of SOA and gas-phase products formed in
518 the Paul Scherrer Institute (PSI) 27 m³ Teflon chamber from low (10 ppb) and high (40 ppb) initial
519 α -pinene concentration were exposed to OH by TME ozonolysis and HONO photolysis at an RH
520 of approximately 50 % (Tritscher et al. 2011). An OH concentration of 2×10^6 to 10×10^6 molecules
521 cm⁻³ was maintained up to four hours. The authors reported an additional 50 % SOA mass forming

522 after aging using the first-order, size-independent particle wall-loss correction for the suspended
523 organic mass concentration measured by AMS. An increase of 0.04 in the oxygen to carbon ratio
524 was also observed during aging.

525 In the 84.5 m³ Aerosol Interaction and Dynamics in the Atmosphere (AIDA) aluminum
526 chamber at Karlsruhe Institute of Technology, an OH concentration of 2×10^6 to 10×10^6 molecules
527 cm⁻³ was used by a constant flow of TME (dark aging). The authors observed an increase of 17-
528 55 % in the SMPS-derived SOA mass concentration (density corrected) after aging during four
529 experiments with initial α -pinene concentration ranging from 14 to 56 ppb (Salo et al., 2011). In
530 the 270 m³ Simulation of Atmospheric Photochemistry in a large Reaction (SAPHIR) Teflon
531 chamber at Forschungszentrum Jülich, SOA and vapors generated from the ozonolysis of 40 ppb α -
532 pinene was aged for three consecutive days with OH produced by ambient light chemistry. An OH
533 concentration of $2\text{-}5 \times 10^6$ molecules cm⁻³ was maintained and 9 %, 4 % and 1 % additional SOA
534 was formed respectively after aging each day. These values were corrected for particle wall loss
535 using different wall-loss rate constants determined during different periods of the experiment.

536 Our result of 20-40 % additional SOA formation due to aging is well within the range of
537 that from the above chambers. The difference in the results from each chamber could potentially
538 be attributed to different OH exposure (e.g. a constant flow of HONO or TME was provided in the
539 PSI chamber). Other plausible explanations include whether the reported values were particle wall-
540 loss corrected and whether the same method was adopted for the correction.

541 For the HONO aging experiment performed in the CMU chamber during the
542 MUCHACHAS campaign, Henry and Donahue (2012) suggested a potentially strong photolysis
543 effect based on decreasing organic to sulfate ratio derived from the AMS measurements. In our
544 experiments, the organic to sulfate ratio was affected by the size-dependent wall-loss process. Both
545 the AMS-measured organic to sulfate ratio and the SMPS-measured OA remained relatively
546 constant after correcting for the size dependence of the particle-wall process in these experiments.
547 We thus conclude that minimum photolysis was observed for our experiments.

548

549 **5. Conclusions**

550 With an OH exposure equivalent to 2-4 days of typical atmospheric oxidation conditions,
551 the OH aging of the α -pinene ozonolysis products formed 20-40 % additional SOA mass for the
552 experimental conditions used in this work. Elevated RH up to 50 % has minimum effect on SOA

553 production due to aging. We have constrained the aging effects on additional SOA formation
554 quantitatively using both SMPS and AMS measurements.

555 A more oxygenated product distribution was observed after aging. A stepwise increase of
556 0.02-0.04 in O:C was observed within half an hour after the first introduction of OH. After the
557 second-generation products were exposed to additional OH, the O:C grew continuously until the
558 end of the experiments with an absolute increase of up to 0.04. During this period, minimum SOA
559 production was observed. We attribute this phenomenon to condensed-phase reactions. Further
560 investigation on a molecular scale is needed.

561 This work essentially explored the additional SOA formation potential of the α -pinene
562 ozonolysis products under high NO_x conditions. The aging time scale of this study of a few days
563 corresponds to the atmospheric lifetime of the corresponding aerosol. The additional formation of
564 SOA observed here is clearly non-negligible, but is also much less than the doubling or tripling of
565 the SOA that has been assumed in few modeling studies (Lane et al., 2008) which resulted in
566 overprediction of the biogenic SOA. The present results can be used for the improvements of the
567 currently used parameterizations for the aging of α -pinene SOA products in CTMs.

568
569
570
571 *Acknowledgement:* The work was funded by the EPA STAR grant 835405 and the EUROCHAMP-
572 2020 EU project.

574 6. References

- 575 Atkinson, R., and Arey J.: Atmospheric degradation of volatile organic compounds, Chemical
576 Reviews, 103, 4605-4638, 2003.
- 577 Barnet, P., Dommen, J., DeCarlo, P. F., Tritscher, T., Praplan, A. P., Platt, S. M., Prévôt A. S.
578 H., Donahue, N. M., and Baltensperger, U.: OH clock determination by proton transfer
579 reaction mass spectrometry at an environmental chamber, Atmos. Meas. Tech., 5, 647–656,
580 2012.
- 581 Canagaratna, M. R., Jimenez, J. L., Kroll, J. H., Chen, Q., Kessler, S. H., Massoli, P., Hildebrandt
582 Ruiz, L., Fortner, E., Williams, L. R., Wilson, K. R., Surratt, J. D., Donahue, N. M., Jayne,
583 J. T., and Worsnop, D. R.: Elemental ratio measurements of organic compounds using
584 aerosol mass spectrometry: characterization, improved calibration, and implications,
585 Atmos. Chem. Phys., 15, 253-272, 2015.

586 Chacon-Madrid, H. J., Henry, K. M., and Donahue, N. M.: Photo-oxidation of pinonaldehyde at
587 low NO_x: from chemistry to organic aerosol formation, *Atmos. Chem. Phys.*, 13, 3227-
588 3236, 2013.

589 Cocker III, D. R., Flagan, R. C., and Seinfeld, J. H.: State-of-the-art chamber facility for studying
590 atmospheric aerosol chemistry, *Environ. Sci. Technol.*, 35, 2594–2601, 2001.

591 Crump, J. G., and Seinfeld, J. H.: Turbulent deposition and gravitational sedimentation of an
592 aerosol in a vessel of arbitrary shape, *J. Aerosol Sci.*, 2, 405–415, 1981.

593 Davidson, C. I., Phalen, R. F., and Solomon, P. A.: Airborne particulate matter and human health:
594 a review, *Aerosol Science and Technology*, 39, 737–749, 2005.

595 Donahue, N. M., Henry, K. M., Mentel, T. F., Kiendler-Scharr, A., Spindler, C., Bohn, B., Brauers,
596 T., Dorn, H. P., Fuchs, H., Tillmann, R., Wahner, A., Saathoff, H., Naumann, K.-H.,
597 Mohler, O., Leisner, T., Muller, L., Reinnig, M.-C., Hoffmann, T., Salo, K., Hallquist, M.,
598 Frosch, M., Bilde, M., Tritscher, T., Barnet, P., Praplan, A. P., DeCarlo, P. F., Dommen,
599 J., Prevot, A. S. H., and Baltensperger, U.: Aging of biogenic secondary organic aerosol
600 via gas-phase OH radical reactions, *Proc. Natl. Acad. Sci., U.S.A.*, 109, 13503 –13508,
601 2012.

602 Donahue, N. M., Robinson, A. L., Stanier, C. O., and Pandis, S. N.: Coupled partitioning, dilution
603 and chemical aging of semivolatile organics, *Environ. Sci. Technol.*, 40, 2635-2643, 2006.

604 George, I. J., Slowik J., and Abbatt J. P. D.: Chemical aging of ambient organic aerosol from
605 heterogeneous reaction with hydroxyl radicals, *Geophys. Res. Lett.*, 35, L13811, 2008.

606 Griffin, R. J., Cocker, D. R., Seinfeld, J. H., and Dabdub, D.: Estimate of global atmospheric
607 organic aerosol from oxidation of biogenic hydrocarbons, *Geophys. Res. Lett.*, 26, 2721–
608 2724, 1999.

609 Henry, K. M., and Donahue, N. M.: Photochemical aging of α -pinene secondary organic aerosol:
610 effects of OH radical sources and photolysis: *J. Phys. Chem. A*, 116, 5932–5940, 2012.

611 Henry, K. M., Lohaus T., and Donahue, N. M.: Organic aerosol yields from α -pinene oxidation:
612 bridging the gap between first-generation yields and aging chemistry, *Environ. Sci.*
613 *Technol.*, 46, 12347–12354, 2012.

614 Intergovernmental Panel on Climate Change: Climate Change 2007: Synthesis Report.
615 Contribution of Working Groups I, II and III to the Fourth Assessment Report of the
616 Intergovernmental Panel on Climate Change, edited by R. K. Pachauri and A. Reisinger,
617 eds., 104 pp., Cambridge Univ. Press, New York, 2007.

618 Julin, J., Winkler, P. M., Donahue, N. M., Wagner, P. E., and Riipinen, I.: Near-unity mass
619 accommodation coefficient of organic molecules of varying structure, *Environ. Sci.*
620 *Technol.*, 48, 12083–12089, 2014.

621 Kalberer, M., Sax, M., and Samburova, V.: Molecular size evolution of oligomers in organic
622 aerosols collected in urban atmospheres and generated in a smog chamber, *Environ. Sci.*
623 *Technol.*, 40, 5917–5922, 2006.

624 Keywood, M. D., Varutbangkul, V., Bahreini, R., Flagan, R. C., and Seinfeld, J. H.: Secondary
625 organic aerosol formation from the ozonolysis of cycloalkenes and related compounds,
626 *Environ. Sci. Technol.*, 38, 4157–4164, 2004.

627 Krechmer, J. E., Pagonis, D., Ziemann, P. J., and Jimenez, J. L.: Quantification of gas-wall
628 partitioning in Teflon environmental chambers using rapid bursts of low-volatility oxidized
629 species generated in situ, *Environ. Sci. Technol.*, 50, 5757–5765, 2016.

630 Kostenidou E., Pathak R. K., and Pandis S. N.: An algorithm for the calculation of secondary
631 organic aerosol density combining AMS and SMPS data; *Aerosol Science and Technology*,
632 41, 1002–1010, 2007.

633 [Kuwata, M., Zorn S. R., and Martin S. T.: Using elemental ratios to predict the density of organic](#)
634 [material composed of carbon, hydrogen, and oxygen, *Environ. Sci. Technol.*, 46, 787-794,](#)
635 [2012.](#)

636 Lambe, A. T., Miracolo, M. A., Hennigan, C. J., Robinson, A. L., and Donahue, N. M.: Effective
637 rate constants and uptake coefficients for the reactions of organic molecular markers (n-
638 alkanes, hopanes and steranes) in motor oil and diesel primary organic aerosols with
639 hydroxyl radicals, *Environ. Sci. Technol.*, 43, 8794–8800, 2009.

640 Lane, T., Donahue, N. M., and Pandis, S. N.: Simulating secondary organic aerosol formation
641 using the volatility basis-set approach in a chemical transport model, *Atmospheric*
642 *Environment*, 42, 7439-7451, 2008.

643 Loza, C. L., Chhabra, P. S., Yee, L. D., Craven, J. S., Flagan, R. C., and Seinfeld, J. H.: Chemical
644 aging of m-xylene secondary organic aerosol: laboratory chamber study, *Atmos. Chem.*
645 *Phys.*, 12, 151–167, 2012.

646 Matsunaga, A., and Ziemann, P. J.: Gas-wall partitioning of organic compounds in a Teflon film
647 chamber and potential effects on reaction product and aerosol yield measurements, *Aerosol*
648 *Science and Technology*, 44, 881–892, 2010.

649 McMurry, P. H., and Rader, D. J.: Aerosol wall losses in electrically charged chambers, *Atmos.*
650 *Chem. Phys.*, 4, 249–268, 1985.

651 Müller, L., Reinnig, M. C., Naumann, K. H., Saathoff, H., Mentel, T. F., Donahue, N. M., and
652 Hoffmann, T.: Formation of 3-methyl-1,2,3-butanetricarboxylic acid via gas phase
653 oxidation of pinonic acid - a mass spectrometric study of SOA aging, *Atmos. Chem. Phys.*,
654 12, 1483–1496, 2012.

655 Nah, T., McVay, R. C., Zhang, X., Boyd, C. M., Seinfeld, J. H., and Ng, N. L.: Influence of seed
656 aerosol surface area and oxidation rate on vapor wall deposition and SOA mass yields: a
657 case study with α -pinene ozonolysis, *Atmos. Chem. Phys.*, 16, 9361–9379, 2016.

658 Ng, N. L., Kroll, J. H., Chan, A. W. H., Chhabra, P. S., Flagan, R. C., and Seinfeld, J. H.: Secondary
659 organic aerosol formation from m-xylene, toluene, and benzene, *Atmos. Chem. Phys.*, 7,
660 3909–3922, 2007.

661 Palm, B. B., Campuzano-Jost, P., Ortega, A. M., Day, D. A., Kaser, L., Jud, W., Karl, T., Hansel,
662 A., Hunter, J. F., Cross, E. S., Kroll, J. H., Peng, Z., Brune, W. H., and Jimenez, J. L.: In
663 situ secondary organic aerosol formation from ambient pine forest air using an oxidation
664 flow reactor, *Atmos. Chem. Phys.*, 16, 2943–2970, 2016.

665 [Paulson, S. E., Chung, M., Sen, A. D., and Orzechowska, G.: Measurement of OH radical](#)
666 [formation from the reaction of ozone with several biogenic alkenes, *J. Geophys. Res.*, 103,](#)
667 [25533-25539, 1998.](#)

668 Pope, C. A., Ezzati, M., and Dockery, D. W.: Fine-particulate air pollution and life expectancy in
669 the United States, *New Engl. J. Med.*, 360, 376-386, 2009.

670 Qi, L., Nakao, S., and Cocker, D. R.: Aging of secondary organic aerosol from α -pinene ozonolysis:
671 Roles of hydroxyl and nitrate radicals, *Journal of the Air & Waste Management*
672 *Association*, 62, 1359–1369, 2012.

673 Robinson, A. L., Donahue, N. M., Shrivastava, M. K., Weitkamp, E. A., Sage, A. M., Grieshop,
674 A. P., Lane, T. E., Pierce, J. R., and Pandis, S. N.: Rethinking organic aerosol: semivolatile
675 emissions and photochemical aging, *Science*, 315, 1259–1262, 2007.

- 676 Salo, K., Hallquist, M., Jonsson, Å. M., Saathoff, H., Naumann, K.-H., Spindler, C., Tillmann R.,
677 Fuchs, H., Bohn, B.; Rubach, F., Mentel, T. F., Müller, L., Reinnig, M., Hoffmann, T., and
678 Donahue, N. M.: Volatility of secondary organic aerosol during OH radical induced ageing;
679 Atmos. Chem. Phys., 11, 11055–11067, 2011.
- 680 Tritscher, T., Dommen, J., DeCarlo, P. F., Gysel, M., Barmet, P. B., Praplan, A. P., Weingartner
681 E., Prévôt, A. S. H., Riipinen, I., Donahue, N. M., and Baltensperger, U.: Volatility and
682 hygroscopicity of aging secondary organic aerosol in a smog chamber, Atmos. Chem.
683 Phys., 11, 11477–11496, 2011.
- 684 Trump, E. R., Riipinen, I., and Donahue, N. M.; Interactions between atmospheric ultrafine
685 particles and secondary organic aerosol mass: a model study, Boreal Environ. Res., 19,
686 352–362, 2014
- 687 Tsimpidi, A. P., Karydis, V. A., Zavala, M., Lei, W., Bei, N., Molina, L., and Pandis, S. N.: Sources
688 and production of organic aerosol in Mexico City: insights from the combination of a
689 chemical transport model (PMCAMx-2008) and measurements during MILAGRO, Atmos.
690 Chem. Phys., 11, 5153–5168, 2011.
- 691 Wang, N., Donahue, N. M., and Pandis, S.N.: Performance of different particle wall-loss correction
692 methods for aging experiments of alpha-pinene SOA in a smog chamber, Aerosol Science
693 and Technology; in preparation.
- 694 Ye, P., Ding, X., Hakala, J., Hofbauer, V., Robinson, E. S., and Donahue, N. M.: Vapor wall loss
695 of semi-volatile organic compounds in a Teflon chamber, Aerosol Science and Technology,
696 50, 822-834, 2016.
- 697 [Ye, P., Ding, X., Ye, Q., and Robinson, E. S.: Uptake of semivolatile secondary organic aerosol
698 formed from \$\alpha\$ -pinene into nonvolatile polyethylene glycol probe particles, J. Phys. Chem.
699 A, 120, 1459-1467, 2016.](#)
- 700 Zhang, Q., Jimenez, J. L., Canagaratna, M. R., Allan, J. D., Coe, H., Ulbrich, I., Alfarra, M. R.,
701 Takami, A., Middlebrook, A. M., Sun, Y. L., Dzepina, K., Dunlea, E., Docherty, K., De-
702 Carlo, P. F., Salcedo, D., Onasch, T., Jayne, J. T., Miyoshi, T., Shimo, A., Hatakeyama,
703 S., Takegawa, N., Kondo, Y., Schneider, J., Drewnick, F., Borrmann, S., Weimer, S.,
704 Demerjian, K., Williams, P., Bower, K., Bahreini, R., Cottrell, L., Griffin, R. J., Rautiainen,
705 J., Sun, J. Y., Zhang, Y. M., and Worsnop, D. R.: Ubiquity and dominance of oxygenated
706 species in organic aerosols in anthropogenically-influenced Northern Hemisphere
707 midlatitudes, Geophys. Res. Lett., 34, L13801, 2007.
- 708 Zhang, X., Cappa, D. C., Jathar, S. H., McVay, R. C., Ensberg, J. J., Kleeman, M. J., and Seinfeld,
709 J. H.: Influence of vapor wall loss in laboratory chambers on yields of secondary organic
710 aerosol, PNAS, 111, 5802-5807, 2014.

711
712
713
714

715

716

717

718

720

721

Table 1: Initial conditions of the α -pinene ozonolysis aging experiments.

722

Experiment	α-pinene (ppb)	O₃ (ppb)	Initial seed surface area ($\mu\text{m}^2 \text{cm}^{-3}$)	RH (%)	OH^a ($\times 10^7$ molecules cm^{-3})	OH introduction time (h after α- pinene consumption)
1	33	450	850	<20	2.4	0.3
2	14	600	760	<20	2.7	0.8
3	35	450	720	<20	2.0	1.1
4	16	500	950	<20	2.4 ^b	1.1
5	20	400	710	~50	2.7	0.8

723

724 ^aThe OH concentration was calculated using the decay of butanol-d9 (monitored by PTRMS)
725 (Barnet et al., 2012).

726 ^bEstimated OH concentration for Exp. 4 based on the other experiments. The PTRMS data was
727 not available during that time for Exp. 4.

728

729

730

731

732

733

734

735

736

737

738

739

740

741

742

743

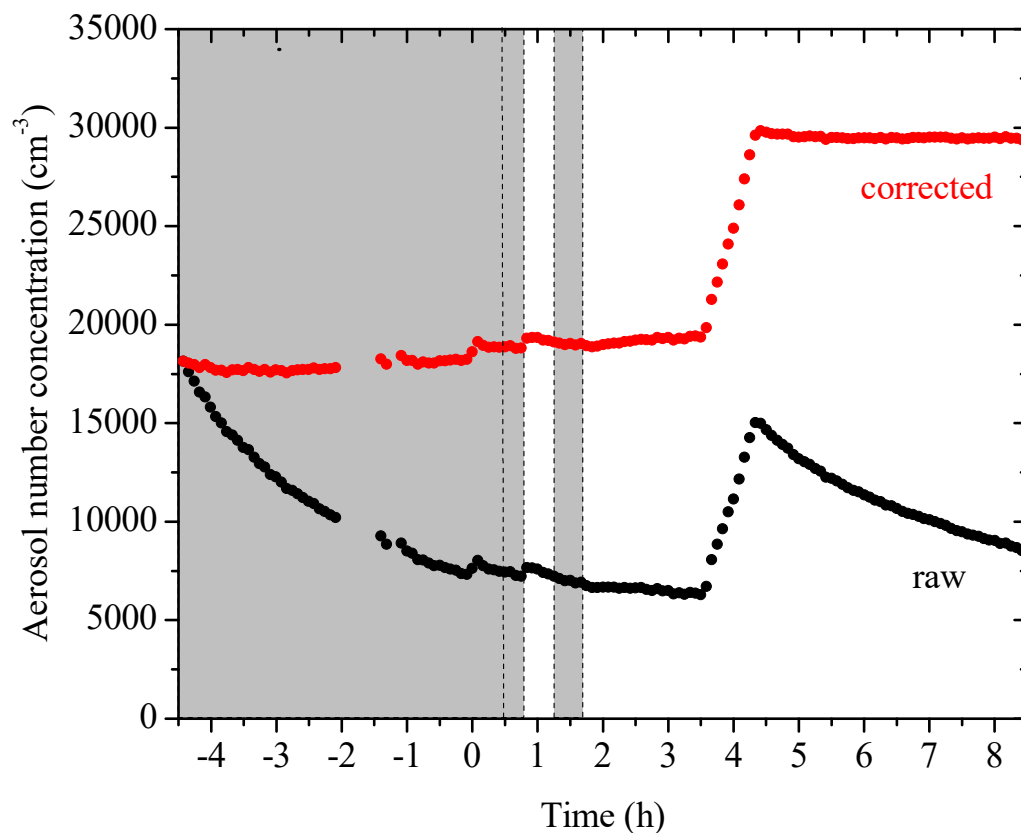
744

745
746
747
748

Table 2: SOA mass concentration and yields of the α -pinene ozonolysis aging experiments.

Experiment	$C_{\text{SOA},1}$ ($\mu\text{g m}^{-3}$)	Y_1 (%)	$C_{\text{SOA},2}$ ($\mu\text{g m}^{-3}$)	Y_2 (%)	ΔOA (%)	$\Delta[\text{Org/Sulf}]$ (%)
1	37.7 \pm 1.6	20.6 \pm 0.9	48.8 \pm 2.0	26.7 \pm 1.1	29.4 \pm 6.9	27.0 \pm 5.8
2	16.7 \pm 0.9	21.5 \pm 1.2	18.3 \pm 1.0	23.5 \pm 1.3	19.8 \pm 8.1	18.1 \pm 2.9
3	57.1 \pm 1.3	29.4 \pm 0.7	71.0 \pm 1.6	36.2 \pm 0.8	23.5 \pm 3.6	19.1 \pm 3.6
4	16.8 \pm 0.6	19.1 \pm 0.6	20.8 \pm 0.7	23.7 \pm 0.8	24.0 \pm 5.3	21.9 \pm 2.1
5	22.2 \pm 0.7	19.5 \pm 0.6	25.4 \pm 0.8	22.3 \pm 0.7	20.5 \pm 4.7	21.2 \pm 4.4

749
750
751
752
753
754
755



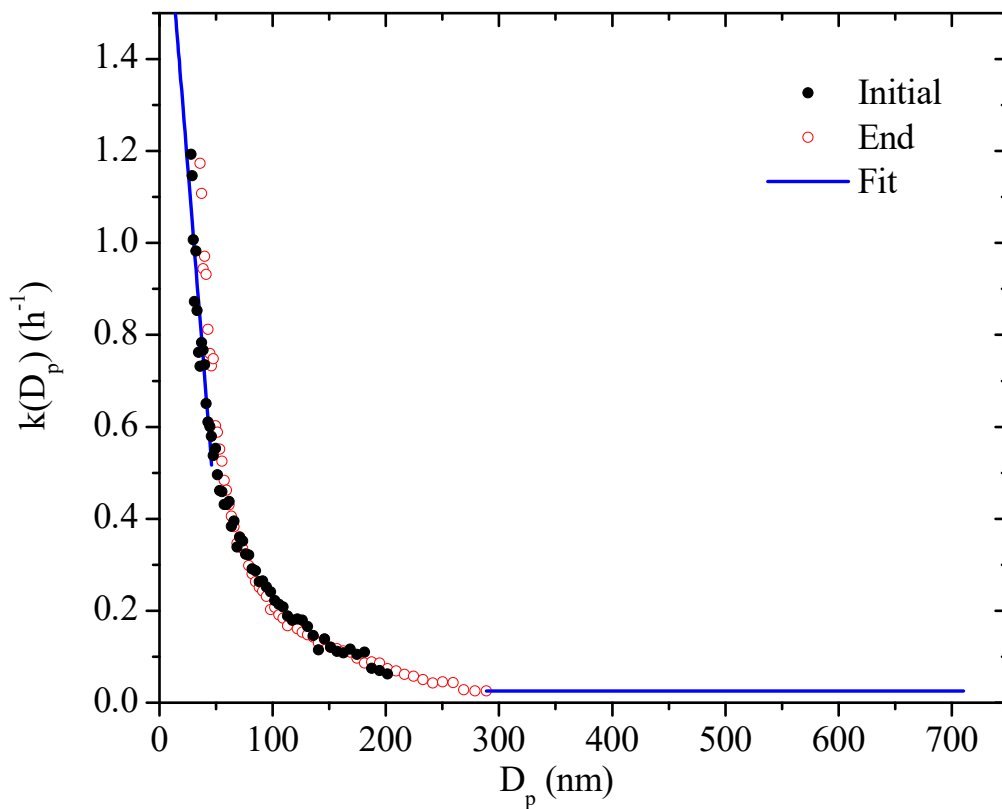
756

757 **Figure 1:** SMPS-measured (black symbols) and the size-dependent particle wall-loss corrected
 758 (red symbols) aerosol number concentration evolution during a typical experiment (Exp. 1). Ozone
 759 was added into the chamber at time zero to initiate α -pinene ozonolysis. The shaded areas indicate
 760 that the chamber was dark. The dashed lines mark the beginning and the end of the two times
 761 HONO were added, respectively. The increase in number concentration at $t=3.5$ h is due to the
 762 injection of 5 g L^{-1} ammonium sulfate particles. An additional 100 cm^{-3} particles were formed due
 763 to nucleation both at the ozonolysis step and the aging step. Data were not recorded from $t=-2$ h
 764 to -1.4 h.

765

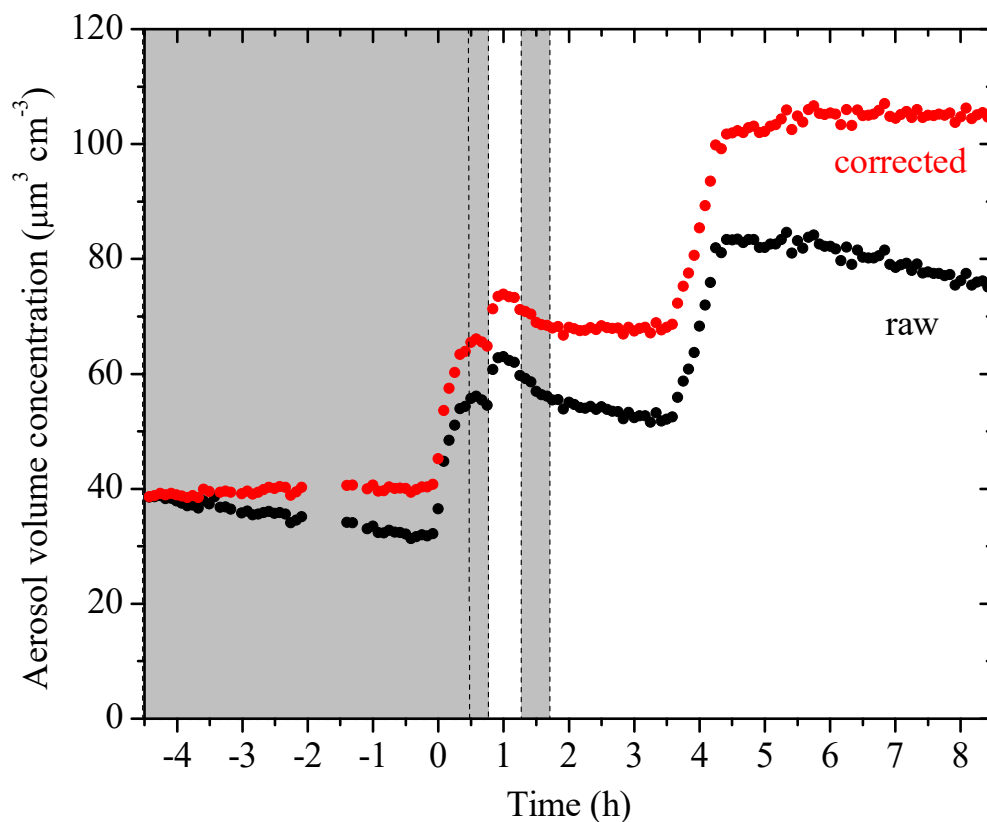
766

767



768
 769 **Figure 2:** The size-dependent particle wall-loss rate constant profile, $k(D_p)$, for Exp. 1. The black
 770 symbols are the rate constants calculated based on the wall-loss process of the initial ammonium
 771 sulfate seed particles from $t=-4.5$ h to $t=0$ h, while the red open symbols those that of the additional
 772 ammonium sulfate particles at the end from $t=4.5$ h to $t=8.5$ h. The blue line is the fit determined.

773
 774
 775
 776

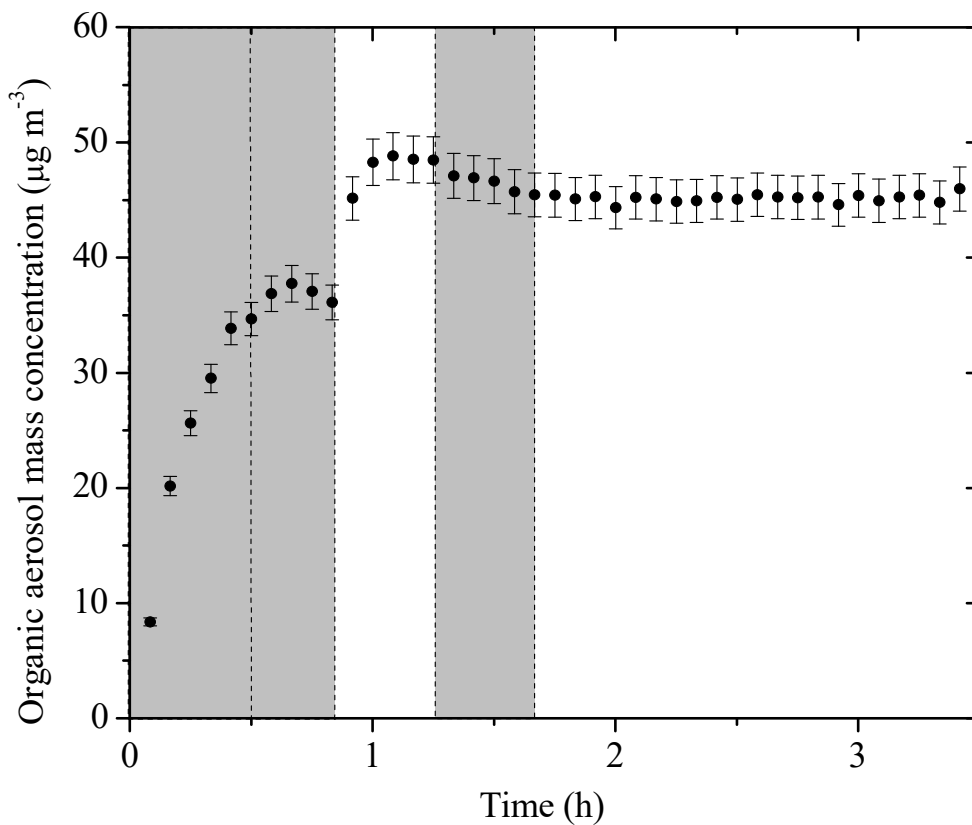


777

778 **Figure 3:** SMPS-measured (black symbols) and the size-dependent particle wall-loss corrected
 779 (red symbols) aerosol (seed and organic) volume concentration evolution during a typical
 780 experiment (Exp. 1). Ozone was added into the chamber at time zero to initiate α -pinene ozonolysis.
 781 The shaded areas indicate that the chamber was dark. The dashed lines mark the beginning and the
 782 end of the two times HONO were added, respectively. 5 g L^{-1} ammonium sulfate particles were
 783 injected into the chamber at $t=3.5 \text{ h}$. Data were not recorded from $t=-2 \text{ h}$ to -1.4 h .

784

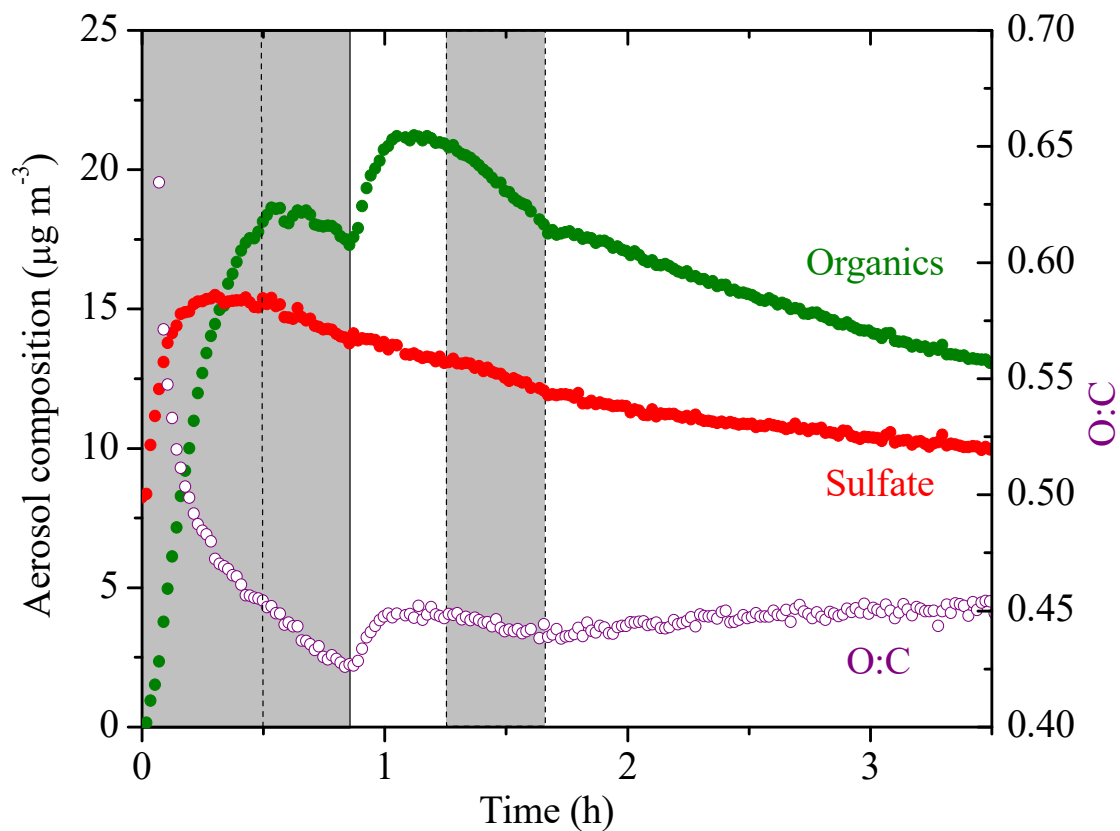
785



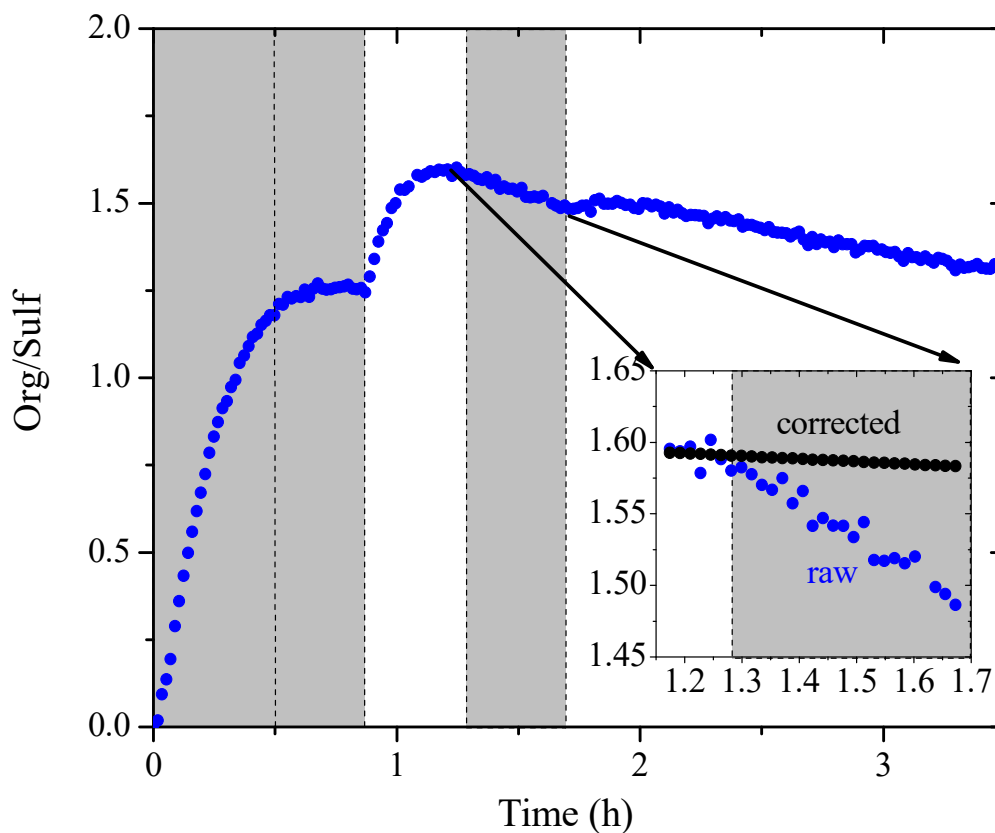
786
787

788 **Figure 4:** The particle wall-loss corrected SOA mass concentration ($\rho=1.4 \text{ g cm}^{-3}$) evolution for
 789 Exp. 1 derived from SMPS measurements. The corresponding error shown is due to the particle
 790 wall-loss correction. Ozone was added into the chamber at time zero to initiate α -pinene ozonolysis.
 791 The shaded areas indicate that the chamber was dark. The dashed lines mark the beginning and the
 792 end of the two times HONO were added, respectively.

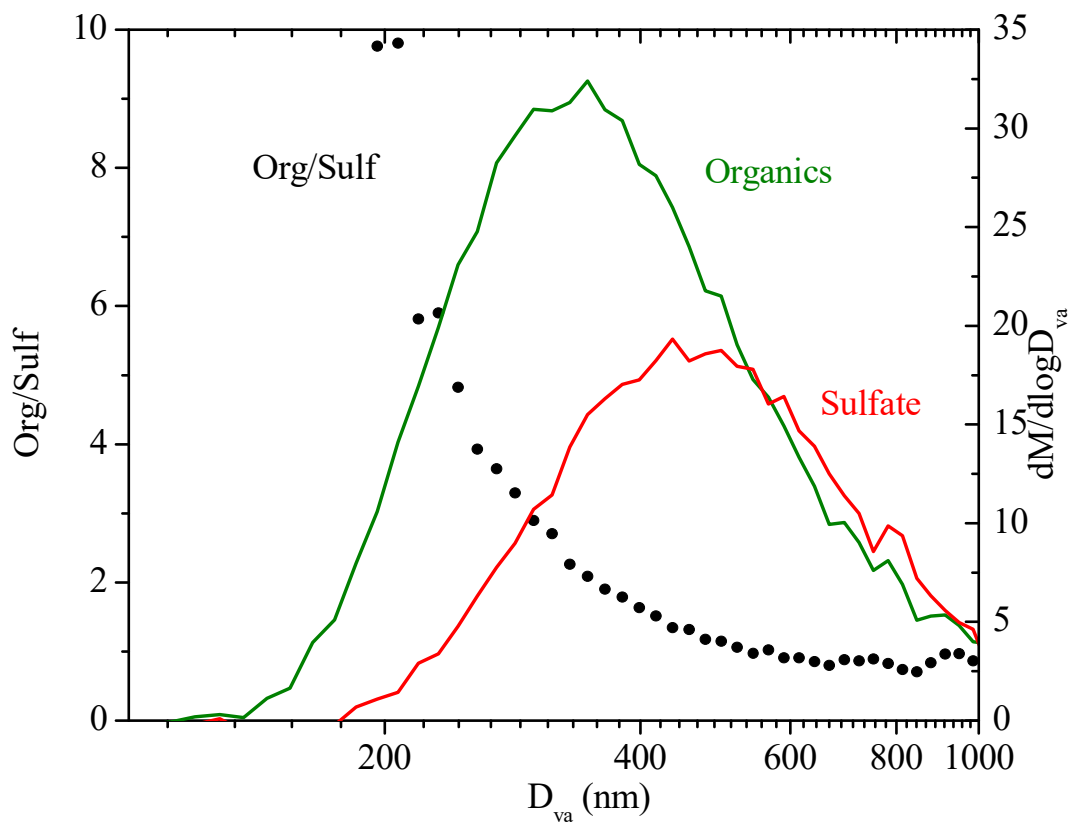
793
794
795
796
797



798
 799 **Figure 5:** The AMS-measured aerosol composition (CE=1) (left axis) and the atomic oxygen to
 800 carbon ratio (right axis) evolving with time for Exp. 4. The increase in the sulfate signal at $t=0$ is
 801 the result of a change in the collection efficiency (CE). Ozone was added into the chamber at time
 802 zero to initiate α -pinene ozonolysis. The shaded areas indicate that the chamber was dark. The
 803 dashed lines mark the beginning and the end of the two times HONO were added, respectively.



804
 805 **Figure 6:** The AMS-derived organic to sulfate ratio time series for Exp. 1. The inset is a blow-up
 806 of the Org/Sulf ratio from its maximum until the second time when the UV lights were turned on.
 807 The black symbols are the particle wall-loss corrected Org/Sulf during that half hour. Ozone was
 808 added into the chamber at time zero to initiate α -pinene ozonolysis. The shaded areas indicate that
 809 the chamber was dark. The dashed lines mark the beginning and the end of the two times HONO
 810 were added, respectively.



811

812 **Figure 7:** The dependence of the AMS-derived organic to sulfate ratio on particle vacuum
 813 aerodynamic diameter for Exp. 1 (left axis). Also shown are the AMS-measured organic (green)
 814 and sulfate (red) mass distribution (right axis). The results are based on PToF data averaged over
 815 ~2.5 hours ($t=1.1$ h to 3.5 h).

816

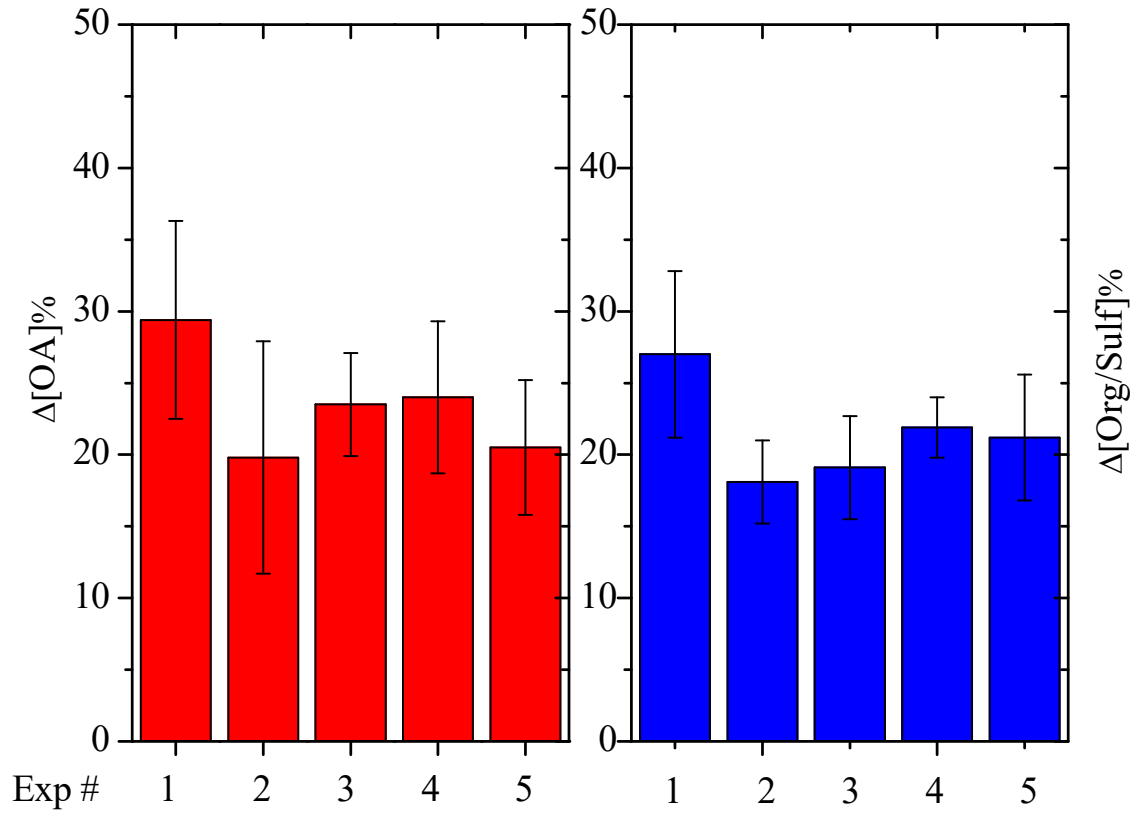
817

818

819

820

821



822

823

824 **Figure 8:** SMPS-derived percent change in the particle wall-loss corrected SOA (red columns)
 825 mass concentration after aging and AMS-derived percent change in organic to sulfate ratio (blue
 826 columns) after aging for all five experiments.

827

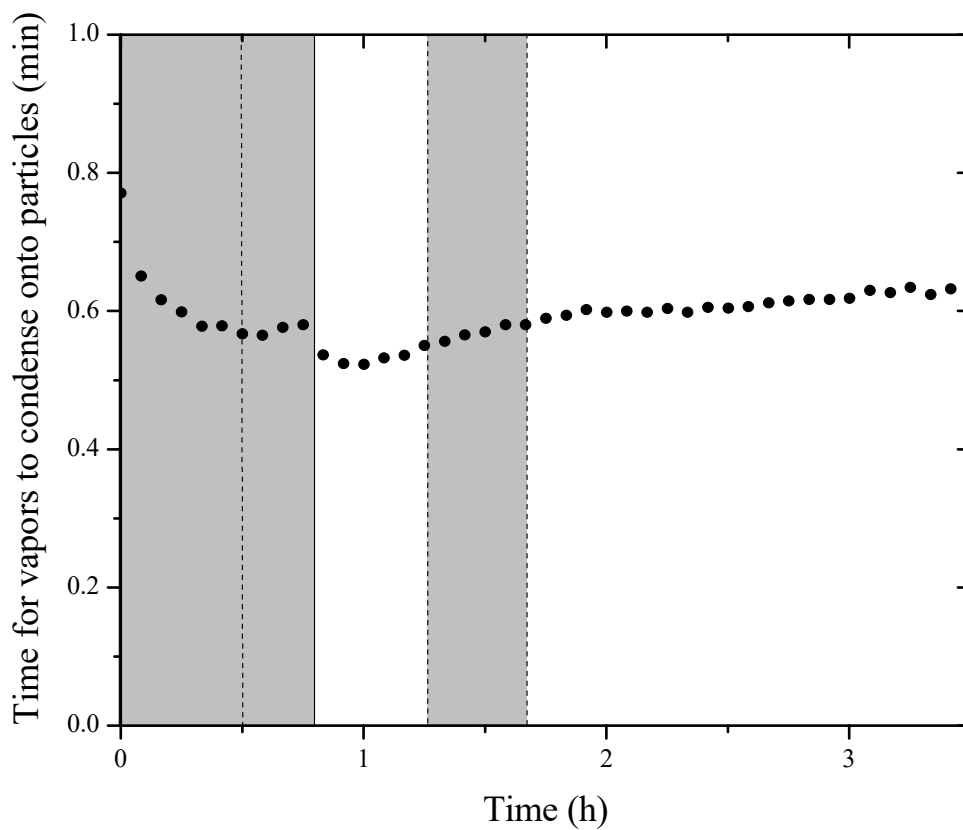
828

829

830

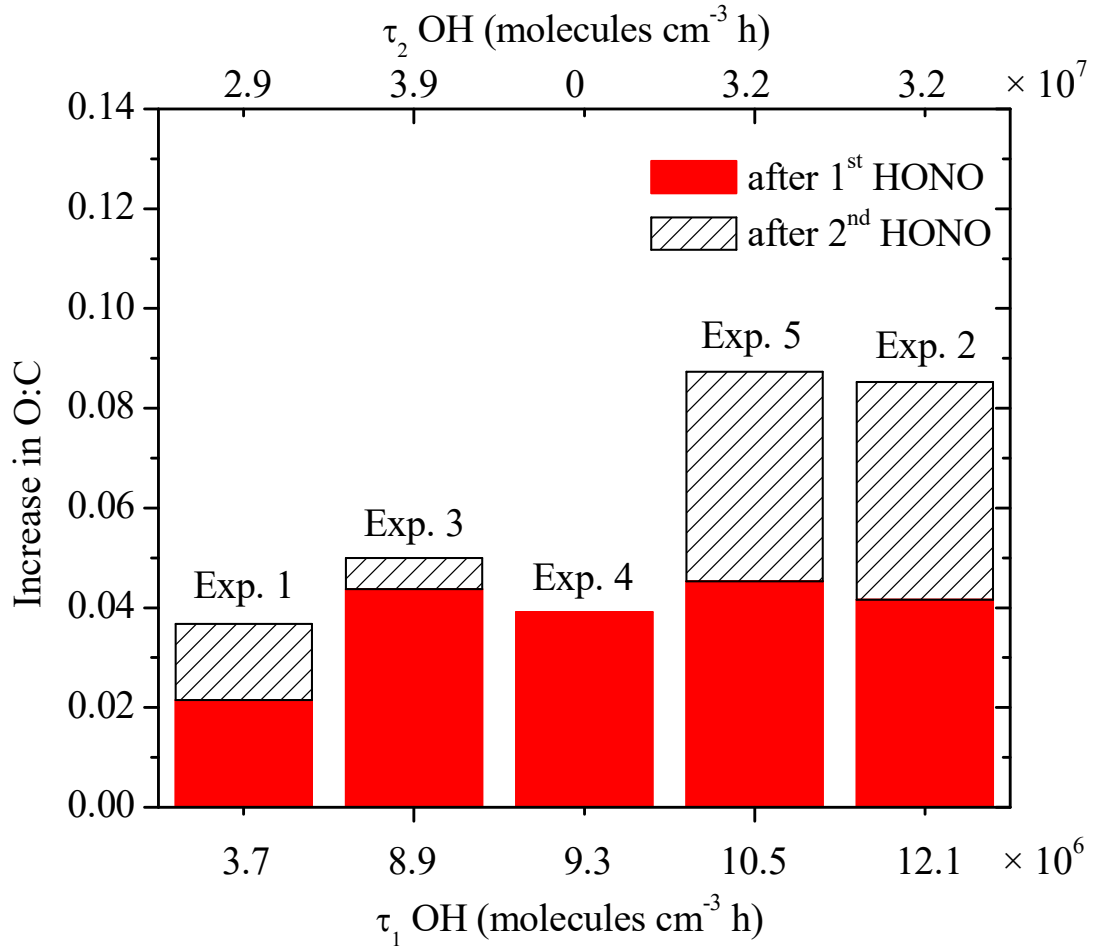
831

832



833

834 **Figure 9:** The calculated condensation sink (CS) in the form of time scale for vapors condensing
 835 onto particles (1/CS). Ozone was added into the chamber at time zero to initiate α -pinene
 836 ozonolysis. The shaded areas indicate that the chamber was dark. The dashed lines mark the
 837 beginning and the end of the two times HONO were added, respectively.



838

839

840 **Figure 10:** The absolute increase in O:C after the two doses of OH, respectively, with the
 841 corresponding exposure. The solid red columns are the increase in O:C after the first introduction
 842 of OH, with the corresponding exposure on the bottom axis. The hatched columns are the increase
 843 in O:C after the second introduction of OH, with the corresponding exposure on the top axis.

844

845

846

847

848

849

850